

**FABRICATION OF POLYMER NANOFIBER / POLY (3,4
ETHYLENE DIOXYTHIOPHENE) / METAL PARTICLE
HYBRID COMPOSITE FOR VOLATILE ORGANIC
COMPOUND SENSING APPLICATIONS**

**A Thesis Submitted to
the Graduate School of
Izmir Institute of Technology
in Partial Fulfillment of the Requirements for the Degree of**

MASTER OF SCIENCE

in Chemistry

**by
Irem ACAR**

**July 2020
IZMIR**

ABSTRACT

FABRICATION OF POLYMER NANOFIBER / POLY (3,4 ETHYLENE DIOXYTHIOPHENE) / METAL PARTICLE HYBRID COMPOSITE FOR VOLATILE ORGANIC COMPOUND SENSING APPLICATIONS

This study aims to produce polymer nanofiber / poly (3, 4 ethylene dioxythiophene) / metal particle hybrid composite as a bioelectronic interface for the detection of volatile organic compounds in human breath. The sensor platform consists of two layers: polymeric nanofiber structure and conductive layer. Polyurethane (PU), polycaprolactone (PCL) and poly L-lactide-co- ϵ -caprolactone (PLLCL) were selected to form polymeric nanofibers with electrospinning. For electrospinning process, solutions of polyurethane (PU) (25wt%) in DMF, polycaprolactone (PCL) (20wt%) in DCM (4) - DMF (1) and poly L-lactide-co- ϵ -caprolactone (PLLCL) (10wt%) in DCM (9) -DMF (1) are prepared. PU, PCL and PLLCL polymer solutions are subjected to 25 kV, 29kV and 25 kV electrical potential, respectively, to produce electrospinning fibers. Poly(3,4-ethylenedioxythiophene) (PEDOT) and multi-walled carbon nanotubes (MWCNTs) are used to produce conductive layers on PU, PCL and PLLCL polymer nanofibers. The produced sensor platforms are tested by the electrochemical station, which records the electrical current change over time. The sensing mechanism is assumed to be the adsorption of VOCs to the conductive PEDOT and CNT layer, thus blocking the electron current on the PEDOT and CNT network and causing resistance change. More clearly; swelling of the polymer structure in the sensor causes destruction in the upper layer and micro-dimensional cracks in the PEDOT and CNT network, increasing resistance to electron flow and decreasing current. Organic volatile compounds (acetone, toluene, ethanol, isopene etc.) are detected from ppm to ppb range and reproducible and reliable responses are recorded.

ÖZET

UÇUCU ORGANİK BİLEŞİK ALGILAMA UYGULAMALARI İÇİN POLİMER NANOFİBER / POLİ (3,4 ETİLEN DİOKSİTTİOFEN) / METAL PARÇACIK HİBRİT KOMPOZİT ÜRETİMİ

Bu çalışma, insan nefesindeki uçucu organik bileşiklerin saptanması için bir biyoelektronik arayüz olarak polimer nanofiber / poli (3,4 etilen dioksitiofen) / metal parçacık hibrid kompozit üretmeyi amaçlamaktadır. Sensör platformu iki katmandan oluşur: polimerik nanofiber yapı ve iletken katman. Elektroğirme metodu ile polimerik nanofiberler oluşturmak için poliüretan (PU), polikaprolakton (PCL) ve poli L-laktit-ko-p-kaprolakton (PLLCL) seçilmiştir. Elektroğirme yöntemi için polimer çözeltileri şu şekilde hazırlanmıştır: PU (wt 25%) + DCM-DMF, PCL (wt 20%) + DCM-DMF ve PLLCL (wt 10%) + DCM-DMF. PU, PCL ve PLLCL polimer çözeltileri, elektrospun fiberler üretmek için sırasıyla 25 kV, 29kV ve 25 kV elektrik potansiyeline maruz bırakılır. Poli (3,4-etilendioksitiofen) (PEDOT) ve çok duvarlı karbon nanotüpler (MWCNT'ler), PU, PCL ve PLLCL polimer nanofiberleri üzerinde iletken katmanlar üretmek için kullanılır. Üretilen sensör platformları, zaman içindeki elektrik akımı değişimini kaydeden elektrokimyasal istasyon tarafından test edilir. Algılama mekanizmasının, VOC'lerin iletken PEDOT ve CNT katmanına adsorpsiyonu olduğu varsayılır, böylece PEDOT ve CNT ağı üzerindeki elektron akımını bloke eder ve direnç değişikliğine neden olur. Daha açık bir şekilde; sensördeki polimer yapısının şişmesi, PEDOT ve CNT ağında üst katman ve mikro boyutlu çatlaklara zarar vererek elektron akışına karşı direnci artırır ve akımı azaltır. Organik uçucu bileşikler (aseton, toluen, etanol, izopen vb.) ppm ila ppb aralığında tespit edilir ve tekrarlanabilir ve güvenilir tepkiler kaydedilir.

TABLE OF CONTENTS

LIST OF FIGURES.....	iv
LIST OF TABLES	vii
CHAPTER 1. INTRODUCTION	1
1.1. Scope of Thesis	1
1.2. Volatile Organic Compounds.....	1
1.2.1. Gas Chromatography.....	2
1.2.2. Selected-Ion Flow Tube/Mass Spectrometry (SIFT/MS).....	3
1.2.3. Gas Sensor	4
1.3. Conjugated Polymers	5
CHAPTER 2. MATERIALS METHODS	7
2.1. Materials	7
2.2. Fabrication of Polymer-PEDOT:PSS and Carbon Nanotube (CNT) Sensors.....	7
2.2.1. Preparation of PMMA Substrate	7
2.2.2. Electrospinning	8
2.2.3. Fabrication of Polymer Nanofibers on PMMA Substrate	8
2.2.4. Sensor Modification	10
2.2.5. Printed Circuit Board Fabrication	11
2.2.6. Electrical Characterization	11
CHAPTER 3. RESULTS AND DISCUSSION.....	13
3.1. Characterization of The Sensor Platform.....	13
3.1.1. Nanofibers Characterization.....	13
3.1.2. Surface Characterization of MWCNT and PEDOT:PSS.....	22
3.2. Electrical Characterization of PU-PCL-PLLCL Gas Sensors.....	24
CHAPTER 4. CONCLUSIONS	33

REFERENCES.....34

LIST OF FIGURES

<u>Figure</u>	<u>Page</u>
Figure 1. Schematic diagram of a gas chromatograph	2
Figure 2. Schematic diagram of a SIFT/MS	3
Figure 3. Molecular structures of extensively studied conjugated polymers	5
Figure 4. Chemical structure of PEDOT:PSS	6
Figure 5. Bare and copper tape functionalized PMMA substrates	8
Figure 6. Digital image of (a) electrospun free-standing nanofibers and (b) electrospinning instrument.....	10
Figure 7. Stage of fabrication sensor.....	10
Figure 8. Stage of the sample holder designed from the printed circuit board.....	11
Figure 9. Digital images of (a) Electrical characterization system that measures the response of sensor platforms to volatile organic compound (b) Fully insulated specimen mounting cap enabling connection between the specimen and instrument (c) Glass container designed for volatile organic compound measurements. One gas inlet and outlet fountain, one sheathed organic volatile gas addition chamber (d) Sample holder made of printed circuit board	12
Figure 10. SEM images of polyurethane nanofibers at 10000x: (a) 170 mm, 24 kV, 2.2 ml/hr (b) 175 mm, 29.5 kV, 2.2 ml/hr (c) 200 mm, 24 kV, 2.2 ml/hr (d) 200 mm, 29.5 kV, 2.2 ml/hr	15
Figure 11. SEM images of Polyurethane nanofibers at 5000x: (a) 170 mm, 25 kV, 2 ml/hr (b) 200 mm, 25kV, 2 ml/hr (c) 170 mm, 29 kV, 2 ml/hr (d) 200 mm, 29 kV, 2ml/hr.....	15
Figure 12. SEM images of Polyurethane nanofibers at 5000x: (a) 170 mm, 25 kV, 2 ml/hr (b) 200 mm, 25kV, 2 ml/hr (c) 170 mm, 29 kV, 2 ml/hr (d) 200 mm, 29 kV, 2 ml/hr.....	16
Figure 13. SEM images of PCL nanofibers produced by electrospinning technique on aluminum foil (a) at 250x (b) at 1000x	18

<u>Figure</u>	<u>Page</u>
Figure 14. SEM images of PCL nanofibers at 10000x: (a) 150 mm, 21 kV, 6 ml/hr (b) 150 mm, 23 kV, 6 ml/hr (c) 150 mm, 24 kV, 6 ml/hr (d) 19 mm, 24 kV, 6 ml/hr.....	18
Figure 15. SEM images of PCL nanofibers at 10000x: (a) 120 mm, 19 kV, 2 ml/hr (b) 150 mm, 19 kV, 2 ml/hr (c) 120 mm, 23 kV, 2 ml/hr (d) 150 mm, 23 kV, 2 ml/hr.....	19
Figure 16. SEM images of PCL nanofibers at 10000x: (a) 170 mm, 24 kV, 3 ml/hr (b) 170 mm, 29 kV, 3 ml/hr (c) 170 mm, 24 kV, 6 ml/hr (d) 170 mm, 29 kV, 6 ml/hr.....	21
Figure 17. SEM images polymer nanofibers of (a) - (b) PU, (c) - (d) PCL and (e) – (f) PLLCL	21
Figure 18. SEM images of the PU-MWCNT drop casted device.....	22
Figure 19. SEM images of the PCL-MWCNT drop casted device.....	23
Figure 20. SEM images of the PLLCL-MWCNT drop casted device	23
Figure 21. SEM images of the PU-PEDOT:PSS drop casted device.....	23
Figure 22. SEM images of the PCL-PEDOT:PSS drop casted device.....	24
Figure 23. SEM images of the PLLCL-PEDOT:PSS drop casted device.....	24
Figure 24. VOC responses of PU-CNT sensor exposed (a) to acetone (b) to ethanol.....	25
Figure 25. VOC responses of PCL-CNT sensor exposed (a) to acetone (b) to ethanol.....	25
Figure 26. VOC responses of PLLCL-CNT sensor exposed (a) to acetone (b) to ethanol	25
Figure 27. VOC responses of PU-PEDOT:PSS sensor exposed (a) to acetone (b) to ethanol	27
Figure 28. VOC responses of PCL-PEDOT:PSS sensor exposed (a) to acetone (b) ethanol	27
Figure 29. VOC responses of PLLCL-PEDOT:PSS sensor exposed (a) acetone (b) ethanol.....	27
Figure 30. Humid environment acetone response of bare MWCNT, AuNP doped MWCNT and FeNP doped MWCNT sensors in (a) 30%, (b) 50%, and (c) 70% humid environment	28

<u>Figure</u>	<u>Page</u>
Figure 31. Humid environment ethanol response of bare MWCNT, AuNP doped MWCNT and FeNP doped MWCNT sensors in (a) 30%, (b) 50%, and (c) 66% humid environment	28
Figure 32. Humid environment toluene response of bare MWCNT, AuNP doped MWCNT and FeNP doped MWCNT sensors in (a) 30%, (b) 50%, and (c) 70% humid environment	29
Figure 33. Humid environment hexane response of bare MWCNT, AuNP doped MWCNT and FeNP doped MWCNT sensors in (a) 30%, (b) 50%, and (c) 70% humid environment	30
Figure 34. Humid environment isoprene response of bare MWCNT, AuNP doped MWCNT and FeNP doped MWCNT sensors in (a) 30%, (b) 50%, and (c) 70% humid environment.....	30
Figure 35. Humid environment chloroform response of bare MWCNT, AuNP doped MWCNT and FeNP doped MWCNT sensors in (a) 30%, (b) 50%, and (c) 70% humid environment.....	31
Figure 36. Humid environment acetone response of bare PEDOT, Au doped PEDOT and FeNP doped PEDOT sensors in (a) 30%, (b) 50%, and (c) 70% humid environment	33
Figure 37. Humid environment ethanol response of bare PEDOT, AuNP doped PEDOT and FeNP doped PEDOT sensors in (a) 30%, (b) 50%, and (c) 70% humid environment	33

LIST OF TABLES

<u>Table</u>	<u>Page</u>
Table 1. General information about chemicals used during nano fiber production	9
Table 2. Tried electrospinning parameters of PU and PCL.....	13
Table 3. Electrospinning parameters of PU, PCL and PLLCL.....	21

CHAPTER 1

INTRODUCTION

1.1. Scope of the Thesis

A low cost and portable sensor is designed to detect volatile organic compounds in the breath. The unique candidates for sensor technology Poly(3,4-ethylenedioxythiophene) - poly(styrenesulfonate) (PEDOT: PSS) and carbon nanotube (CNT) conductive polymers are used. The response of the produced sensors to volatile organic compounds is investigated. Sensing properties are investigated against two different polymers and changed by doping gold (Au) and iron (Fe) metal nanoparticles (NPs) to these polymers. The stability of the sensors is also tested.

1.2. Volatile Organic Compounds

Linus Pauling confirmed in 1971 that human breath was a volatile mixture containing more than 250 different VOCs. Volatile organic compounds are chemicals with high vapor pressure and low molecular weight. Human breath contains many volatile organic compounds such as acetone, ethanol, toluene etc. The major VOCs of healthy human breath, acetone (1.2-900 ppb), ethanol (13-1.000 ppb), methanol (160-2000 ppb), isoprene (12-580 ppb), ammonia, and pentane and higher alcohol, aldehyde and ketone components, including small chains (Fenske, Jill D.; Paulson, Suzanne E., 1999). Detection of these volatile organic compounds, which are defined as biomarkers in exhaled breath, is important for the diagnosis of some metabolic diseases (diabetes, asthma etc.) (Righettoni, et al., 2015; Güntner et al., 2019) and some types of cancer (lung cancer) (G. Peng, Tisch, Adams, et al., 2009). Organic volatile compounds such as toluene and hexane, for example, are at levels 1-20 parts-per-billion (ppb) in healthy human breath, while those in lung cancer patients are at levels 10-100 ppb (Peng et. al.,

2010; Konvalina et. al., 2014).

Thus, by selective detection of the change in concentration of these compounds, healthy and sick human can be distinguished.

In this context, gas chromatography and mass spectroscopy methods which can measure VOCs with high sensitivity are available.

1.2.1. Gas Chromatography (GC)

Gas chromatography is a popular technique used to detect organic volatile compounds in human breath. The technique is characterized by a low detection limit (LOD), which enables the identification and quantitation of VOCs present in trace amounts in exhaled breath (S.E. Stein, 1999).

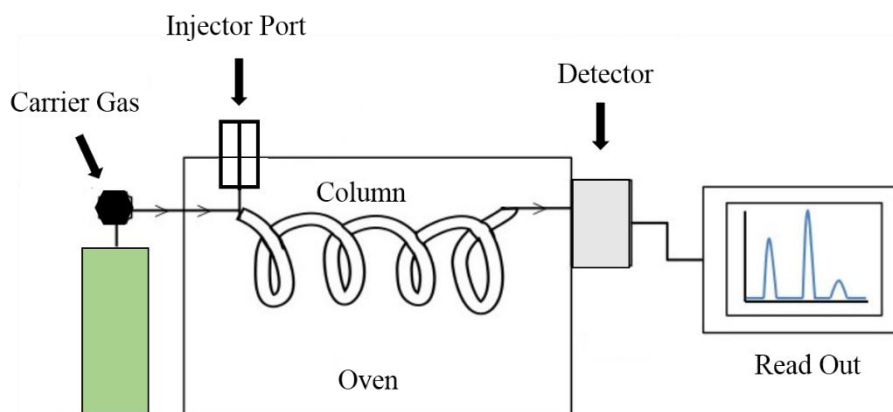


Figure 1. Schematic diagram of a gas chromatograph

Gas chromatography basically consists of 4 main parts: carrier gas, sample injection, chromatographic column and detectors.

Carrier gas: Depending on the detector type, the carrier gas selected must be an inert gas such as nitrogen, argon and helium.

Sample injection: The sample is given evaporated. Injection type and sample size are important for effective separation so the injection port should be above boiling point of the least volatile compounds in analyte.

Chromatographic column: In this section, separation begins and the most important parameter for separation is column temperature. There are two general types of columns, packaged and capillaries.

Detectors: There are many types of detectors that can be used. Each different detector has different selectivity. The choice of detector is chosen depending on the type and purpose of the sample. The main features of the detector: fast response, repeatability, sensitivity, resistance to high temperature, etc.

1.2.2. Selected-Ion Flow Tube/Mass Spectrometry (SIFT/MS)

Selected ion flow tube mass spectrometry (SIFT-MS), along a stream tube in a well-defined chemical ionization of volatile compounds by selected positive ions during a time period containing trace gas analysis trace for a pioneer quantitative mass spectrometry technique.

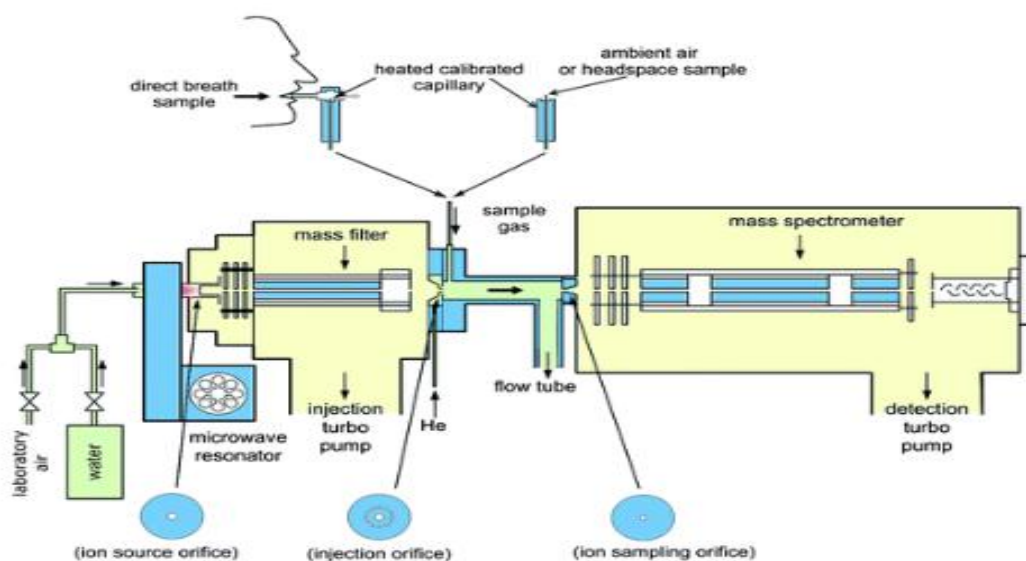


Figure 2. Schematic diagram of a SIFT/MS

(source:<http://www.sift-ms.com/>)

These two techniques mentioned above are suitable for breath analysis. However, these devices are complex and trained personnel are required for their use. For this reason, "sensors based on nanomaterial" take attention for breath analysis.

1.2.3. Gas Sensor

The sensor is a device that converts non-electrical signals such as temperature, humidity and blood pressure into electrical outputs.

Gas sensors have many uses in our daily life in recent years. Over the past decade, gas detection has become increasingly important for different areas, including detection of food degradation, (Galstyan et. al., 2018; ,Pavase et. al., 2018)) human health, (Broza et. al., 2018; Jalal et. al., 2018) and environmental pollution. (Woellner et. al., 2018; Fang et. al., 2018).

Why nanomaterial in sensors? Nanomaterials such as nanoparticles and carbon nanotubes are notable in gas sensor applications due to their proper gas sensing properties. Nanomaterials have a very high surface area for a given volume (M. Meyyappan, 2016). The large surface area leads to high adsorption rates for gases. This can cause rapid changes in some measurable properties of the sensor material, such as resistance, capacitance, or dielectric constant (M. Meyyappan, 2016).

Gas sensors are a low-cost, easiness of use, portability and simpler method than GC and MS based techniques (Corrado Di Natale et. al., 2014; Marco Righettoni et. al., 2015). The gas sensor contains a sensing active layer which is sensitive to conductivity. The interaction between the gas molecules and the materials takes place mainly on the surface. Therefore, the number of atoms present on the surface of a material is critical to control sensor performance. Designed as a breath analyzer, these sensors need to meet some requirements. Firstly, sufficient sensitivity and lower detection limit (their detection limit is in the units of ppm and ppb range) are required to detect respiratory markers at trace level concentrations (Andreas T. Guntner et. al., 2019; Corrado Di Natale et. al., 2014). In addition, the sensor must have a high selectivity to accurately detect single breath marks against other compounds. Finally, the stability of the sensor is important throughout the working time to provide reproducible breath analysis (Vaddiraju, S., Gleason, K. K., 2010).

Polymer-metal nanoparticle hybrids, obtained by assembling metal nanoparticles onto the surfaces of conductive polymer nanofibers, allow selective detection of volatile organic compounds (Vaddiraju, S., Gleason, K. K., 2010). In this context, the aim of this study is to develop a sensing platform by coating conductive polymer solutions (PEDOT:PSS and CNT) on polymer nanofibers (PLLCL, PCL and PU) created by electrospinning. It was doped with gold (Au) and iron (Fe) nanoparticles to alter the organic volatile compound retention capacities and selectivity of the sensors produced.

1.3. Conjugated Polymers

Structures containing a π system in the polymer framework are called conjugated polymers. The carbon atoms forming the polymer skeleton form three sigma bonds with adjacent atoms. The remaining p orbitals are connected to the π system. Conducting polymers contain π electron system. The π electron system is responsible for properties such as electrical conductivity, high electron affinity, and optical transitions.

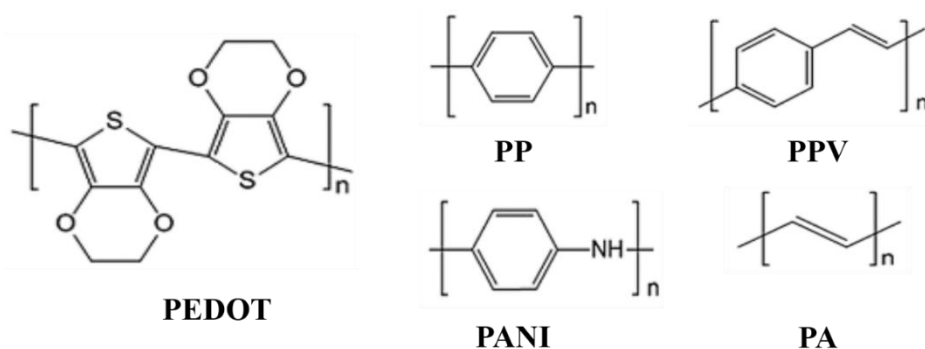


Figure 3. Molecular structures of extensively studied conjugated polymers

Since conductive polymers change properties by merger of ions and solvents (the easiest property change to measure is conductivity), it is possible to develop ion-specific sensors based on conductive polymers. Conducting polymers could allow the incorporation of sensors into clothing. Conductive polymers change volume depending on their oxidation state. Therefore, it is possible to transmit polymers to convert electrical energy into mechanical work (Mohd Hamzah Harun et al., 2007).

Poly (3,4-ethylenedioxy thiophene) (PEDOT) has an important place among conjugated polymers due to its properties such as its high conductivity, stability and optical transparency in the state of conductivity.

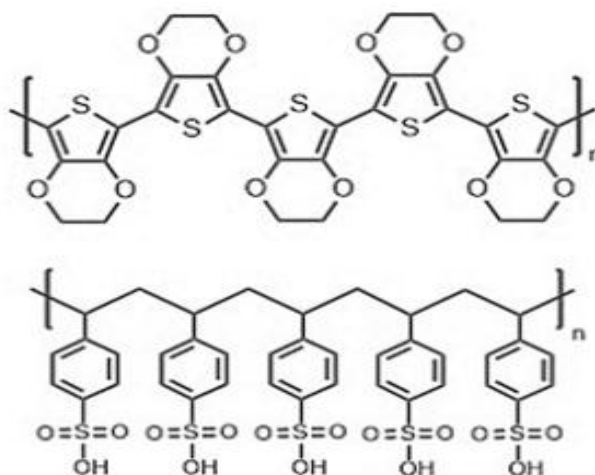


Figure 4. Chemical Structure of PEDOT:PSS.

Because of the insoluble nature of PEDOT in aqueous media, its synthesis with poly (styrenesulfonate) (PSS) forms a well-dispersed aqueous solution. The charges are balanced by incorporating PEDOT chains into the polyanionic PSS matrix. Poly (3,4-ethylenedioxy thiophene): poli (stiren sulfonate) (PEDOT:PSS) is a polymer electrolyte consisting of positively charged conjugated PEDOT and negatively charged saturated PSS. PSS is a polymer surfactant, which helps disperse and stabilize PEDOT in water and other solvents. PEDOT:PSS is the most successful conducting polymer in terms of practical applications.

MWCNT are also part of the gas sensor. The MWCNT material was found in 1991 by Iijima during the production of fullerenes by arc discharge evaporation. MWCNTs are more advantageous in electrical and thermal properties than other carbon materials. Because of these properties, CNTs have wide application area. In particular, high surface to volume ratio and excellent electrical properties that can be easily perturbed with interacting with VOCs (Albanese, Tang, & Chan, 2012). Therefore, MWCNTs are preferred for gas sensors. Additionally, functionalization of MWCNTs with gold (Au) and iron (Fe) metal nanoparticles (NPs) due to its extraordinary catalytic properties, enhance the sensor selectivity and sensitivity considerably (Rao et al., 2017).

CHAPTER 2

MATERIALS & METHODS

2.1. Materials

Poly (L-lactide-co- ϵ -caprolactone) (PLLCL, Resomer Evonik Industries), Polyurethane (PU) (molecular weight of 95,000; cas no 9009-54-5) and Polycaprolactone (PCL, molecular weight of 65,000, Sigma Aldrich; cas no 24980-41-4) were used for fabrication of polymer nanofibers. Dimethylformamide (DMF, $\geq 99\%$, Sigma Aldrich) and, dichloromethane (DCM, $\geq 99\%$, Sigma Aldrich) were used to dissolve polymers. PEDOT: PSS an aqueous suspension (1.3 wt%) were purchased from Sigma-Aldrich. Poly (methyl methacrylate) (PMMA) plate was used for fabrication of sensor. SCP Silver Conductive Paint was purchased from Assemcorp to provide conductivity. Printed circuit board (PCB), copper tape (12 mm x 16 m, 85 μ m thickness) and pin heads purchased. Nitric acid (HNO₃, $\geq 65\%$, Sigma Aldrich), sulfuric acid (H₂SO₄), hydrochloric acid (HCl, $\geq 37\%$, Sigma-Aldrich), and ammonium hydroxide (NH₄OH, 26%, (Sigma-Aldrich)) were used for the functionalization of MWCNTs.

2.2. Fabrication of Polymer-PEDOT:PSS and Carbon Nanotube (CNT)

Sensors

2.2.1. Preparation of PMMA substrate

The PMMA sheet was cut to 400 x 300 mm by Epilog Zing laser engraver via CorelDraw x8. The inner area was carved 1 mm. Reason of cutting PMMA substrate in these sizes; polymer nanofibers obtained with electrospinning provided the best free-standing between poles. Cut settings were set to 30% speed and 60% power.

The two long sides of the prepared PMMA sheet were functionalized with copper tape (in figure 5).



Figure 5. Bare and copper tape functionalized PMMA substrates

2.2.2. Electrospinning

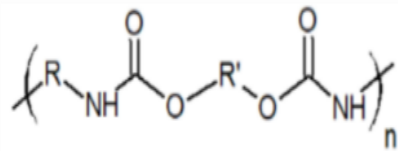
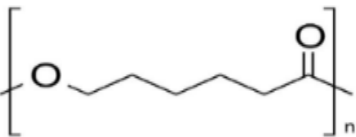
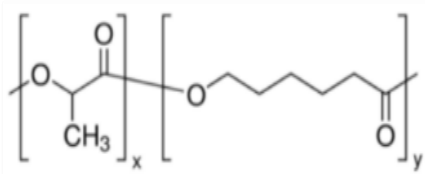
Electrospinning is a method used to produce nanofibers from polymer solutions through electric field. Electrospin method can produce nanofibers in various diameters from nanometers to microns. Electrospinning apparatus consists of a high voltage power supply, a syringe pump, a metallic spinneret and a conductive collector. Electrospinning starts with the electrical charges passing into the polymer solution. The charges push each other to allow the polymer solution to flow in the direction of the electric field. The polymer drop, called Taylor cone, is formed and from this drop the nanofibers are collected on the conductor collector.

2.2.3. Fabrication of Polymer Nanofibers on PMMA Substrate

For fabrication of sensor was used three different polymers (PU (Polyurethane), PCL (Polycaprolactone) and PLLCL (Poly L-lactide-co- ϵ -caprolactone)). In order to produce PU nano fibers, a 15% by weight PU dispersion was prepared by mixing in the presence of DMF solution at 500 rpm for 12 hours. The prepared dispersion was drawn into to a 20 mL capacity syringe and placed in the electrospinning device. The parameters of electrospinning was adjusted as followings; 25 kV voltage, 170 mm nozzle to collector distance, and 2 mL / h flow rate. The collector was set at a constant rotation speed of 500 rpm. The same process was performed in PCL and PLLCL polymers. 20% by weight PCL

dispersion was prepared by stirring in a solvent mixture of DCM / DMF (4: 1) at 500 rpm for 12 hours. The prepared dispersion was transferred to a 20 ml syringe and placed in the electrospinning apparatus. Electrospinning parameters for PCL; 29 kV voltage, 170 mm nozzle to collector distance, 2 mL / h flow rate. To produce PLLCL nanofibers, a 10% by weight dispersion of PLLCL was prepared in a DCM / DMF (9: 1) solvent mixture and stirred for one day on a magnetic stirrer. After the PLLCL was completely dissolved, the 20 ml syringe was filled with polymer solution and connected to the syringe pump of the electrospinning assembly. Electrospinning process was started with the following parameters; 25 kV voltage, 180 mm nozzle to collector distance, 3 mL / h flow rate.

Table 1. General information about chemicals used during nano fiber production

Polymer	Chemical Name	Chemical Structure
PU	Polyurethane	
PCL	Polycaprolactone	
PLLCL	Poly (L-lactic-co-epsilon caprolactone)	

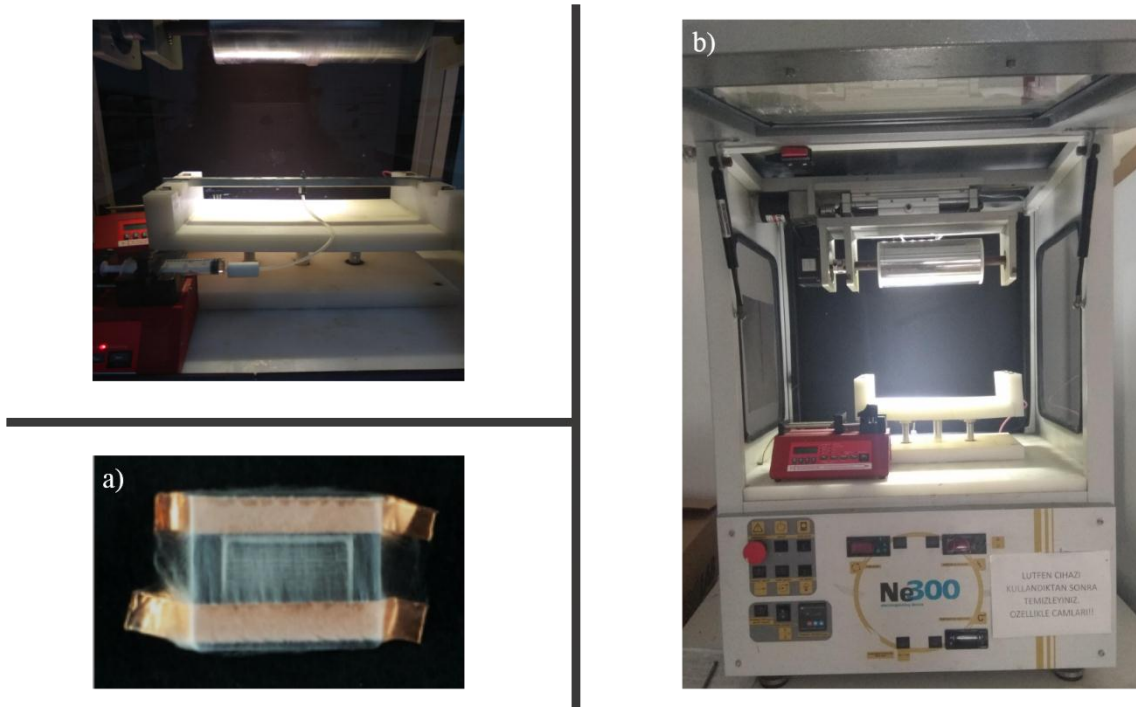


Figure 6. Digital image of (a) electrospun free-standing nanofibers and (b) electrospinning

2.2.4. Sensor Modification

The surface of the sensor was modified with conducting polymers PEDOT: PSS and CNT. For this purpose, drop-casting method was applied. 1.3 % wt. PEDOT: PSS was diluted to 0.2 % with deionized water. A 40 μ l diluted PEDOT: PSS suspension was drop-casted on free-standing PLLCL nanofibers. Then, the prepared PU and PLLCL samples were oven dried at 60 °C for 3 hours. The prepared PCL samples were also dried at 40 °C for 3 hours. The same procedure was performed in CNT. After that, the sensors were placed in the PCB by soldering for electrical characterization.

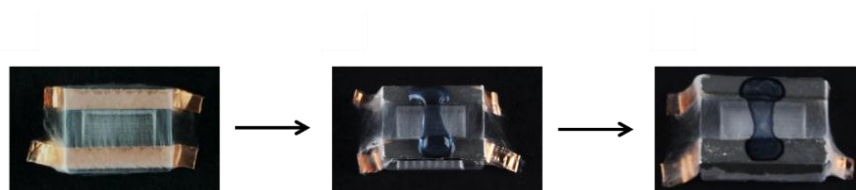


Figure 7. Stage of Fabrication Sensor

2.2.5. Printed Circuit Board Fabrication

PCB was used to investigate the electronic and vapor sensing properties as a conductive platform. The conductive paths designed in the CorelDraw program were printed on coated paper. These conductive paths were transferred to the card at high temperature. The printed circuit board was kept in hydrogen peroxide and hydrochloric acid (1: 3) solution to dissolve the copper parts. The conductive paths isolated with ink were cleaned with the help of acetone. The copper bands on the sensor platform were soldered to the copper paths on the printed circuit board and transmission is provided. Connection between the power supply and the multimeter was provided with gold-pin pins on the printed circuit board. The PCB designed in Figure 8 was shown.

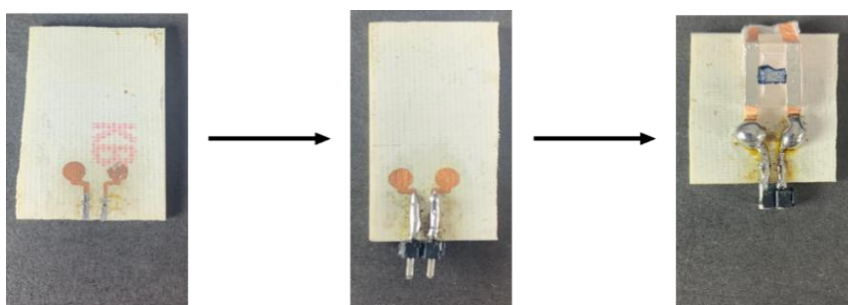


Figure 8. Stages of the sample holder designed from the printed circuit board

2.2.6. Electrical Characterization

The sensors were placed on the printed circuit board and 1V is applied from the power supply (HP 34401A Digital Multimeter). Volatile organic gases were sent to each sensor platform placed in a 1 liter glass container. Then, 0.5 ppm, 5 ppm, 20 ppm, and 100 ppm of volatile organic compound were dropped respectively. The sensors were exposed to volatile organic compounds for 3 minutes. Subsequently, the surface was cleaned with nitrogen gas for 1 minute. Time-dependent current measurements were recorded electronically.

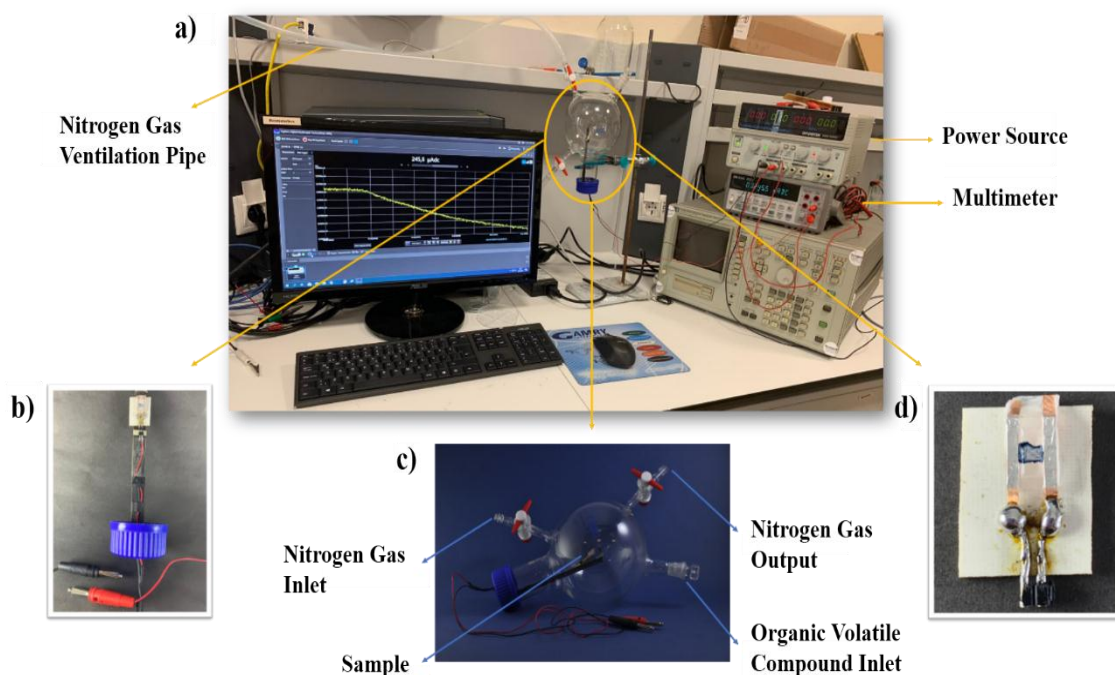


Figure 9. Digital images of (a) Electrical characterization system that measures the response of sensor platforms to volatile organic compounds (b) Fully insulated specimen mounting cap enabling connection between the specimen and instrument (c) Glass container designed for organic volatile compound measurements. One gas inlet and outlet fountain, one sheathed organic volatile gas addition chamber (d) Sample holder made of printed circuit board.

The experimental setup used in Figure 9 was shown in detail. Figure 9- (a) was shown the current change as the response of the sensor exposed to organic volatile compound on the computer screen. Figure 9-(b) was shown the device that provides the connection between the sensor and the device. Figure 9-(c) was shown the glass container designed to provide measurements in a completely isolated environment. On this glass, there was a gas inlet and outlet fountain and a volatile organic volatile gas addition chamber. The sensor was ventilated with nitrogen gas due to the gas inlet and outlet fountain.

CHAPTER 3

RESULT & DISCUSSION

3.1. Characterization of The Sensor Platform

Polyurethane (PU), Polycaprolactone (PCL), and Poly (L-lactide-co-ε-caprolactone) (PLLCL) nanofibers produced by electrospin were characterized by scanning electron microscopy (SEM). Sensor characterization was obtained by multimeter and SEM.

3.1.1. Nanofibers Characterization

Nanofibers obtained by using three different polymers were produced by electrospin technique. Several parameters have been tried to achieve precise fibers for polyurethane (PU) and polycaprolactone (PCL). The tried parameters and optimum parameters for each polymer shown in Table 2.

The ones written in bold were the optimum parameters determined as a result of the trials. SEM images of some samples created with the tried parameters were shared below. The most suitable nanofiber structures were obtained in these parameters. The explanation below was made according to the parameters tried.

Table 2. Tried electrospinning parameters of PU and PCL

Polymer	Specimen	Solution conditions		Spinning conditions		
		Concentration (Wt%)	Solvent composition by volume	Spinning Distance (mm)	Voltage (kV)	Flow rate (mL/h)
	1	8	DMF	170	24	2.2
	2	8	DMF	170	29.5	2.2

(cont. next page)

Tablo 2. (cont.)

PU	3	8	DMF	200	24	2.2	
	4	8	DMF	200	29.5	2.2	
	5	12	DMF	170	25	2	
	6	12	DMF	200	25	2	
	7	12	DMF	170	29	2	
	8	12	DMF	200	29	2	
	9	15	DMF	170	25	2	
	10	15	DMF	200	25	2	
	11	15	DMF	170	29	2	
	12	15	DMF	200	29	2	
	PCL	1	18	Chloroform	150	24	6
		2	15	Acetone	150	21	6
3		15	Acetone	150	23	6	
4		20	Acetone	150	24	6	
5		20	Acetone	170	24	6	
6		20	Acetone	190	24	6	
7		12	DCM(4):Acetone(1)	120	19	2	
8		12	DCM(4):Acetone(1)	150	19	2	
9		12	DCM(4):Acetone(1)	120	23	2	
10		12	DCM(4):Acetone(1)	150	23	2	
11		20	DCM(4):DMF(1)	150	24	3	
12		20	DCM(4):DMF(1)	150	29	3	
13		20	DCM(4):DMF(1)	170	24	3	
14		20	DCM(4):DMF(1)	170	29	3	
15		20	DCM(4):DMF(1)	150	24	6	
16		20	DCM(4):DMF(1)	150	29	6	
17		20	DCM(4):DMF(1)	170	24	6	
18		20	DCM(4):DMF(1)	170	29	6	

Firstly, Polyurethane (PU) nanofibers were made by electrospinning. A solution of polyurethane in dimetilformamid (DMF) solvent was prepared. Prepared concentrations of polyurethane polymer solution were 8%. Applied voltage values and distance changed. Applied values: 24 kV and 29 kV. Distances values: 170 mm and 200 mm. SEM images were as follows:

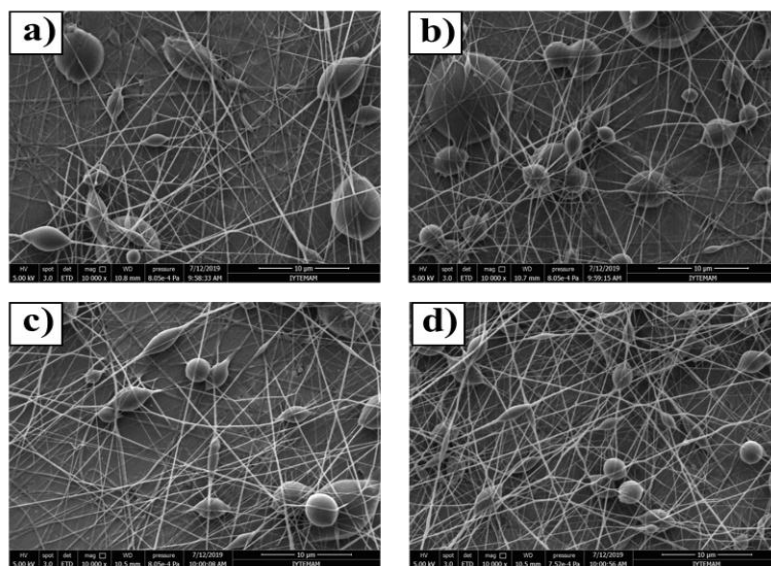


Figure 10. SEM images of Polyurethane nanofibers at 10000x: (a) 170 mm, 24 kV, 2.2 ml/hr (b) 175 mm, 29.5 kV, 2.2 ml/hr (c) 200 mm, 24 kV, 2.2 ml/hr (d) 200 mm, 29.5 kV, 2.2 ml/hr

According to the SEM images shown in figure 10, In the first experiment (8% PU/DMF) a large number of beads were formed. The reason for this was seen as low concentration. So, a solution of polyurethane in dimetilformamid (DMF) solvent was prepared.

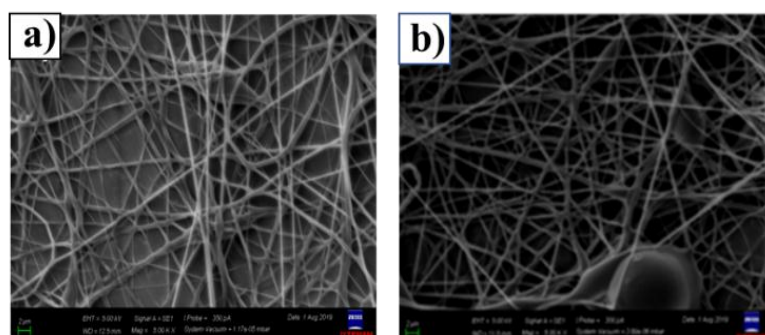
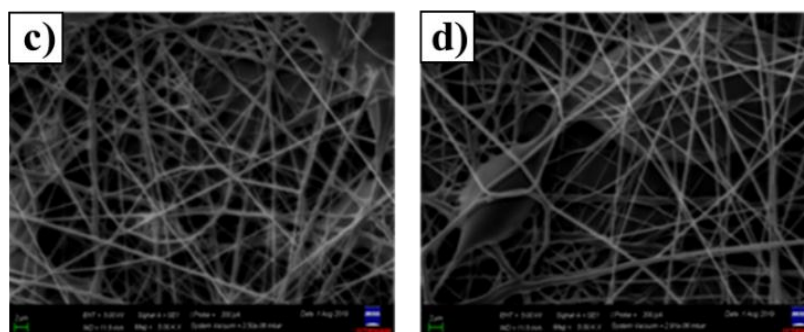


Figure 11. SEM images of Polyurethane nanofibers at 5000x: (a) 170 mm, 25 kV, 2 ml/hr (b) 200 mm, 25kV, 2 ml/hr (c) 170 mm, 29 kV, 2 ml/hr (d) 200 mm, 29 kV, 2 ml/hr.



(Figure 11. cont.)

Firstly, the concentration was increased from 8% to 12%. And 12% Polyurethane polymer Solution was prepared. Electrospinning parameters: The voltages were 25 kV and 29 kV. The flow rate was 2 ml/hr. The collector distances were kept different, 170 mm and 200 mm. SEM images were as in figure 11.

Later, the concentration of polyurethane in DMF was increased from 12% to 15%. And 15% polyurethane polymer solution was prepared. Electrospinning parameters: The voltages were 25 kV and 29 kV. The flow rate is 2 ml/hr. The collector distances were kept different, 170 mm and 200 mm. SEM images were as follows:

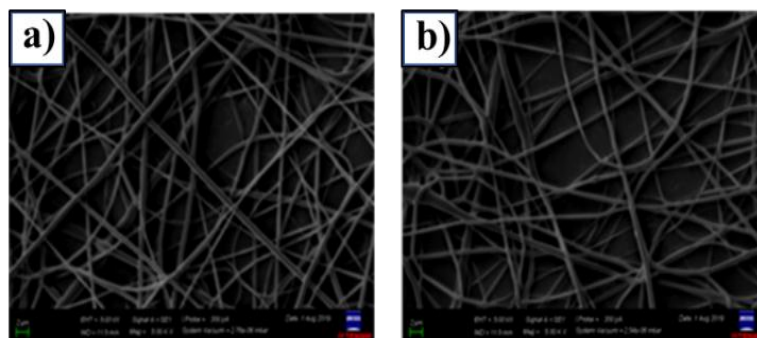
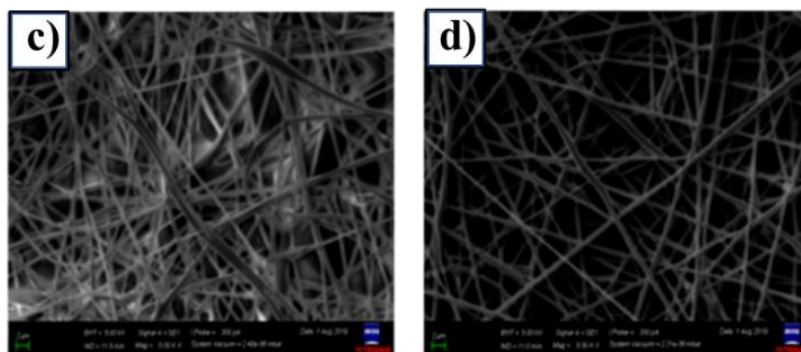


Figure 12. SEM images of Polyurethane nanofibers at 5000x: (a) 170 mm, 25 kV, 2 ml/hr (b) 200 mm, 25kV, 2 ml/hr (c) 170 mm, 29 kV, 2 ml/hr (d) 200 mm, 29 kV, 2 ml/hr.



(Figure 12. Cont.)

The most common problem that occurs in electrospinning was beads. Beads were a result of surface tension forces that overcome forces that support continuous jet elongation (Andray A., 2008). This morphology (beads on a string) was eliminated by increasing the concentration of the polymer. Because, by increasing the polymer concentration in the solution, sufficient chain mixing was ensured and continuous jet elongation was supported. Therefore, solution concentrations were increased in the above parameters. Thus, optimum concentration values were determined without bead deformity and the smallest diameter nanofibers as possible were produced.

The applied voltage value was also critical for electrospinning. High voltage was induced charges in the solution so that the surface tension was exceeded by electrostatic forces in the solution, which was necessary for the initiation of electrospinning (Chen et al., 2012). The applied voltage was seen to have a major effect on nanofiber morphology and diameter. A higher applied voltage results in a thinner fiber diameter. Because of the stronger electric field due to the high voltage applied, it leads to more stress of the polymer jet (Ramakrishna et al., 2005; Lee J. et al., 2004).

After determining the ideal electrospinning parameters for polyurethane (PU), trials were started for poly(ϵ -caprolactone) (PCL). First, solution of PCL in chloroform was tried. 18% polymer solution was prepared. And PCL nanofibers were made by electrospinning. Applied voltage: 24 kV collector distance: 150 mm. . SEM images were below:

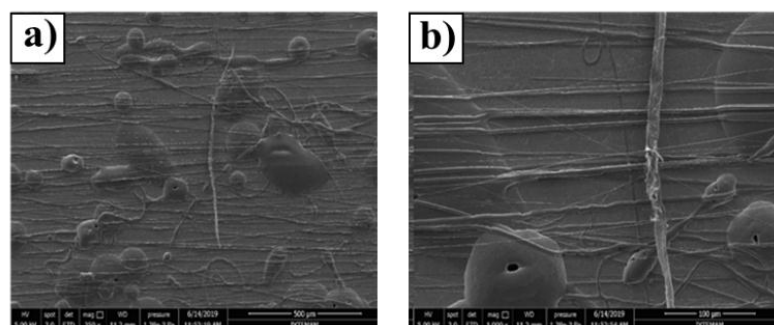


Figure 13. Scanning Electron Microscope images of PCL Nanofibers produced by electrospinning technique on aluminum foil (a) at 250x (b) at 1000x

It was observed that the film structure was formed by electrospinning with prepared PCL in chloroform. For this reason, the chloroform solution used was changed and a new polymer solution was prepared using acetone. A solution of PCL in acetone solvent was prepared. 15% and %20 PCL polymer solutions were prepared. A voltage of 21 kV and 23 kV was applied. The applied flow rate was 6 ml/hr. SEM images were as follows:

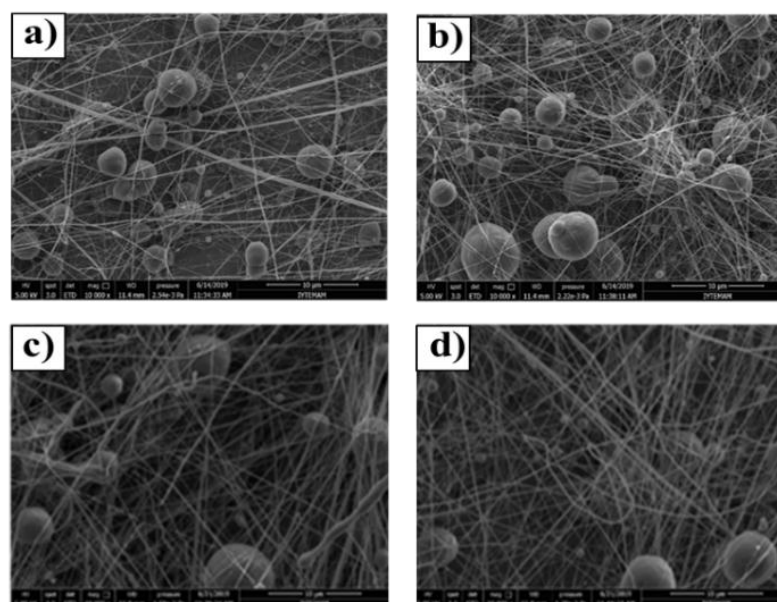


Figure 14. SEM images of Polycaprolactone nanofibers at 10000x: (a) 150 mm, 21 kV, 6 ml/hr (b) 150 mm, 23 kV, 6 ml/hr (c) 150 mm, 24 kV, 6 ml/hr (d) 190 mm, 24 kV, 6 ml/hr

Figure 14 (a) and (b) were shown the 15% solution of PCL in acetone prepared. Fig. 14 (c) ve (d) were demonstrated 20% solution of PCL in acetone. As seen in SEM images, many beads were formed in samples (a) and (b). In samples (c) and (d), where we increase the concentration to destroy these beads, relatively few beads were observed. Despite the numerous spin and solution parameters that were changed and tried, the beads could not be destroyed. So, the PCL polymer solution was tried to prepare in different solvents. The solvent mixture of DCM + Aceton was used for the PCL polymer. A 12% polymer solution was prepared. 19 kV and 23 kV were applied respectively. Collector distance was 120 mm and 150 mm respectively. The flow rate was adjusted to 2 ml / hr.

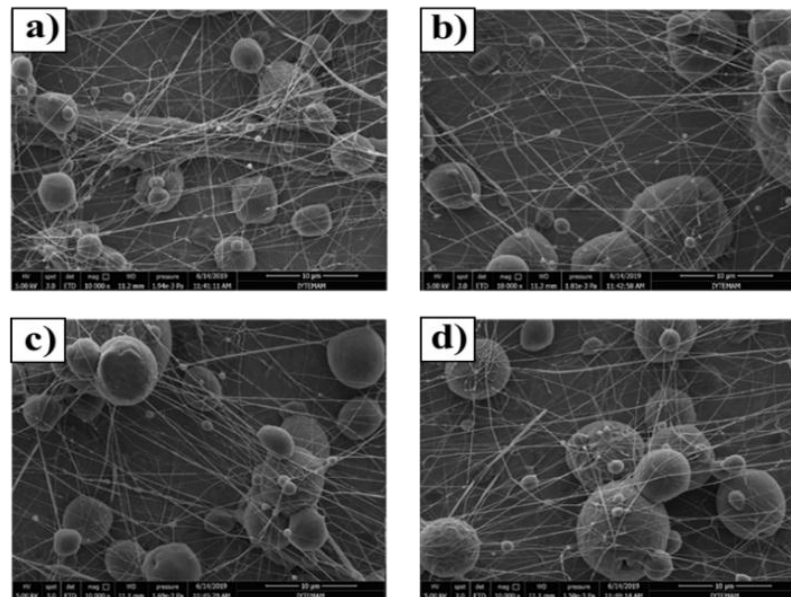


Figure 15. SEM images of Polycaprolactone nanofibers at 10000x: (a) 120 mm, 19 kV, 2 ml/hr (b) 150 mm, 19 kV, 2 ml/hr (c) 120 mm, 23 kV, 2 ml/hr (d) 150 mm, 23 kV, 2 ml/hr

Solvent selection was an important parameter for obtaining bead-free nanofibers. Two important points were noted in the choice of solver: 1) The polymer was completely soluble in solvent. 2) Choosing a solvent with a moderate boiling point. Solvents with a low boiling point cause the jet to dry at the tip of the needle due to the high evaporation rate, and the desired smooth nanofibers can not be obtained. The beads could not be destroyed while PCL nanofibers were being produced, as seen in the SEM images in

Figure 15. The reason for this was that the two solvents (DCM:39.6 °C / Acetone:56 °C) used had low boiling points and therefore very volatile solvents.

Then, the PCL polymer solution was tried to prepare in different solvents. a solution of PCL in DCM/DMF solvent was prepared. The concentration of polymeric solution was %20. Electrospinning parameters: Firstly, the flow rate was kept constant at 3 ml/hr. The applied voltages were 24 kV and 29 kV. The collector distances were kept 170 mm. Images of SEM are shown in figure 12 (a) and (b). Then, the flow rate was increased to 6 ml / hr at the same voltage and distance values. Images of SEM are shown in figure 16 (c) and (d).

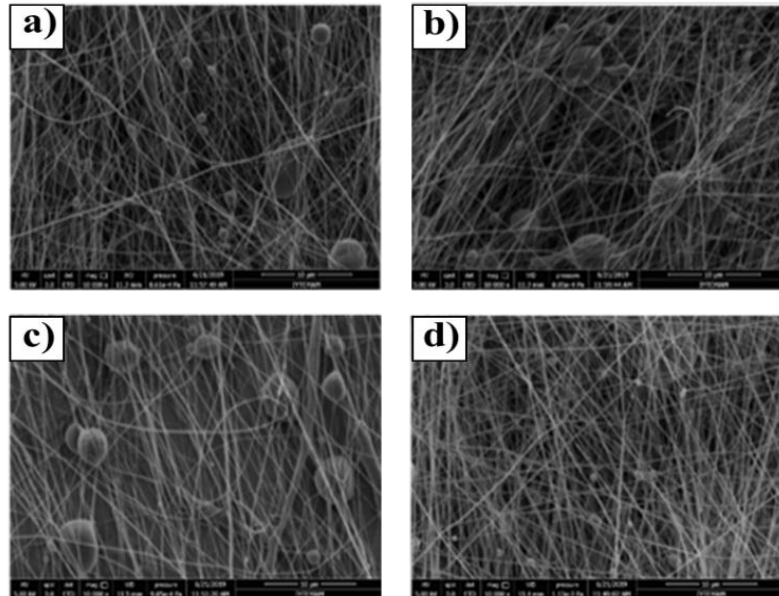


Figure 16. SEM images of Polycaprolactone nanofibers at 10000x: (a) 170 mm, 24 kV, 3 ml/hr (b) 170 mm, 29 kV, 3 ml/hr (c) 170 mm, 24 kV, 6 ml/hr (d) 170 mm, 29 kV, 6 ml/hr

It was then tried by mixing the DMF solvent with DCM, whose boiling point (156 °C) was high relative to DCM. As shown in Figure 16, the beads were significantly reduced in the DCM / DMF solvent mixture. The best results were obtained in the electrospinning parameters of the nanofibers obtained in figure 16- (d). By increasing the flow rate and voltage, the beads were significantly eliminated.

In summary, optimum parameters were also determined for PU and PCL. After that, by making electrospin, PU, PCL and PLLCL nanofiber structures were created in the desired size. The optimum electrospin parameters determined in Table 3 were shown.

Table 3. Electrospinning parameters of PU, PCL, and PLLCL

Polymer	Solution conditions		Spinning conditions		
	Concentration (Wt%)	Solvent composition by volume	Spinning distance (mm)	Voltage (kV)	Flow rate (mL/h)
PU	15	DMF	170	25	2
PCL	20	DCM(4):DMF(1)	170	29	6
PLLCL	10	DCM(9):DMF(1)	180	25	3

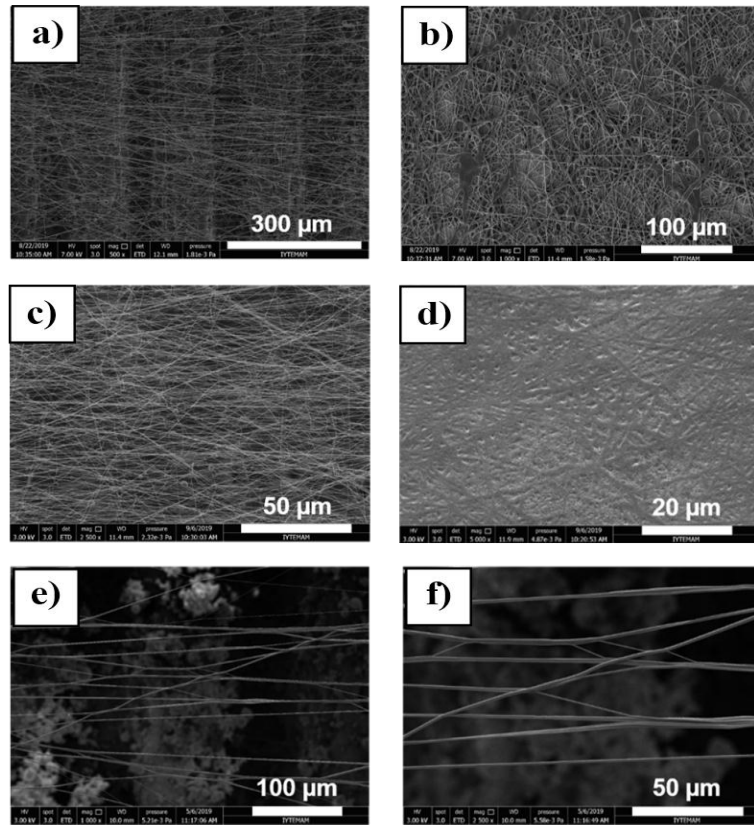


Figure 17. SEM images polymer nanofibers of (a) - (b) PU, (c) - (d) PCL and (e) – (f) PLLCL

In Figure 17, scanning electron microscope images of PU, PCL and PLLCL nanofibers were shared in order taken from the regions between the two copper bands

(a-c-e-f) and on the copper bands (b-d). When the microscope images were examined, PU, PCL and PLLCL nanofibers in the region suspended in the air between the copper bands were sequential, while PU, PCL and PLLCL nanofibers in the region on the copper band were in irregular winding form. This was due to the desire to pull PU, PCL and PLLCL nanofibers to themselves during flight by directing the copper bands electric field to them during the electrospinning process. In this way, PU, PCL and PLLCL nanofibers were drawn towards the electric field concentrated in two copper bands, forming a sequential structure. This bridge - like structure was decidedly important for creating the sensor interface. This was because the bridge-shaped structure has the capacity to carry the conjugated polymer modification of the trickle method on it.

3.1.2. Surface Characterization of MWCNT and PEDOT:PSS

PU, PCL and PLLCL nanofibers formed by electrospinning method were functionalized by drop casting technique with PEDOT: PSS and CNT. High resolution surface images were obtained by scanning electron microscopy (SEM) at different magnifications in order to examine the distribution of the gas sensor platforms on the surface. Figure from 18 to 23 were depicted surface images of the gas sensor platform taken by scanning electron microscope at different magnifications after coating with PEDOT: PSS and CNT on PU, PCL, and PLLCL nanofibers.

Below are the SEM images of the conductive network obtained by impregnating MWCNT into electrospinning PU, PCL and PLLCL nanofiber networks:

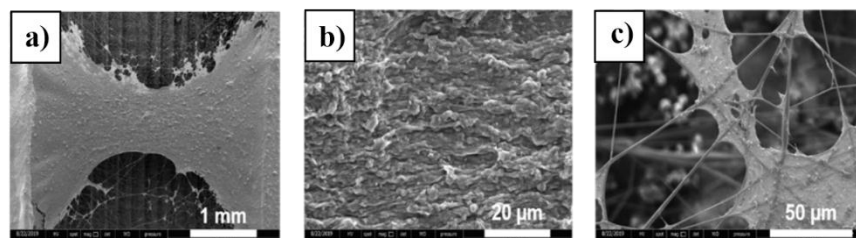


Figure 18. SEM images of the PU-MWCNT drop casted device.

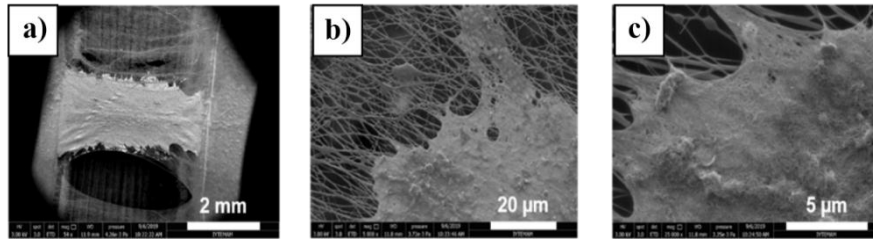


Figure 19. SEM images of the PCL-MWCNT drop casted device.

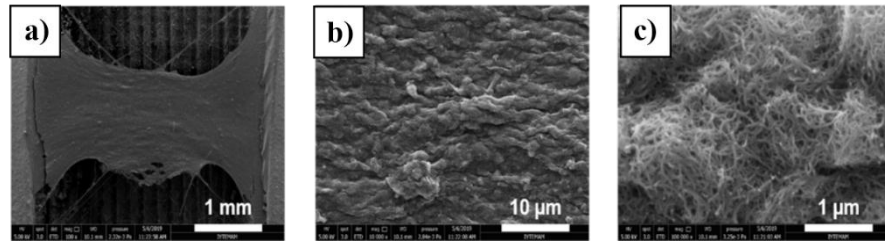


Figure 20. SEM images of the PLLCL-MWCNT drop casted device.

The MWCNT morphology was seen to have a wool-like structure, as seen in the SEM images above. According to the SEM images taken, MWCNT's were entangled and formed a homogeneous film on the surface of the suspended PU, PCL and PLLCL nanofibers. And it covered the entire sensor interface.

Below are the SEM images of the conductive network obtained by impregnating PEDOT:PSS into electrospinning PU, PCL and PLLCL nanofiber networks:

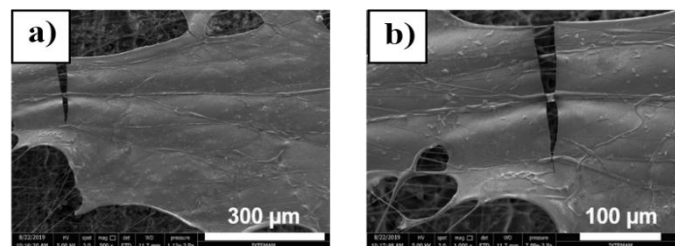


Figure 21. SEM images of the PU-PEDOT:PSS drop casted device

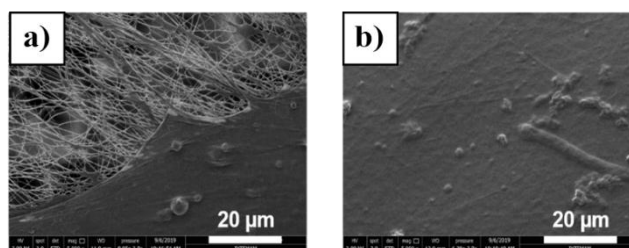


Figure 22. SEM images of the PCL-PEDOT:PSS drop casted device

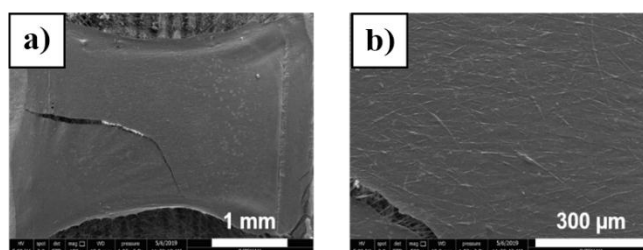


Figure 23. SEM images of the PLLCL-PEDOT:PSS drop casted device

Scanning electron microscope images of PEDOT: PSS polymer coated gas sensors on PU, PCL, and PLLCL nanofibers at different magnifications were shown in Figure 21, 22, and 23. The surface morphology was different from MWCNT. The MWCNT nets had a wool-like structure, while the PEDOT:PSS conductor nets had a smooth morphology. In addition to nanofibers coated with CNT, tear was observed on the surface of nanofibers coated with PEDOT: PSS polymer. This was because when PEDOT: PSS polymer was dripped onto the surface, part of the PEDOT: PSS polymer accumulates on the nano-fibers and some part penetrates the lower part. This irregular distribution was thought to cause cracks and tears on the surface. Due to these tears, the entire sensor interface could not be covered. This was undesirable. Because the gas detection surface area was decreasing.

3.2. Electrical Characterization of PU-PCL-PLLCL Gas Sensors

It was assumed that the detection mechanism of the sensors was caused by adsorption of volatile organic compounds onto the conductive CNT and PEDOT layer. Thus, electron flow in the CNT and PEDOT network was blocked and current exchange

occurred. In simpler terms, the swelling of the polymer structure on the sensor platform caused damage to the upper surface, causing micro-sized reversible cracks in the CNT and PEDOT network, and increased resistance in the electron flow, reducing the current value. The gas sensor thus produced detected organic volatile compounds at the ppm – ppb level in the environment.

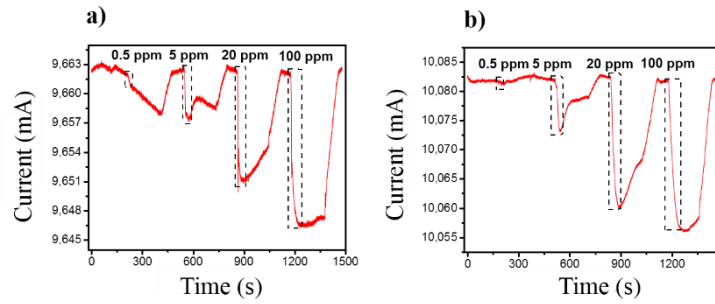


Figure 24. VOC responses of PU-CNT sensor exposed a) to acetone b) to ethanol

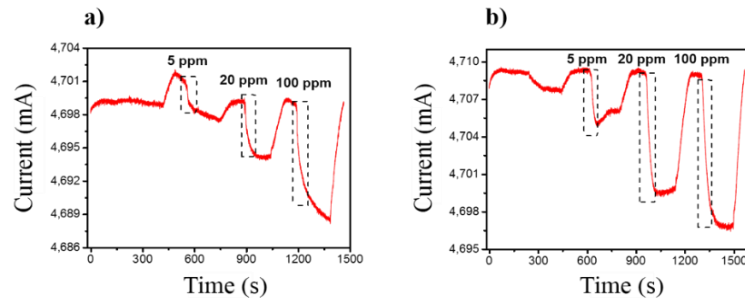


Figure 25. VOC responses of PCL-CNT sensor exposed a) to acetone b) to ethanol

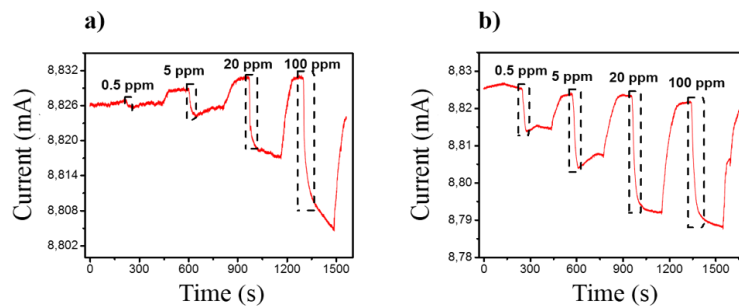


Figure 26. VOC responses of PLLCL-CNT sensor exposed a) to acetone b) to ethanol

Fig. 24, Fig. 25 and Fig. 26 were shown the time-dependent flow graph of the CNT coated sensor exposed to acetone and ethanol gas. When the graphs were examined, when PU-MWCNT, PCL-MWCNT and PLLCL-MWCNT sensors were exposed to organic volatile compounds, the current loss was not observed. It showed that when the analyte was removed by passing nitrogen gas, the sensors returned to their initial baseline signals, and that almost complete desorption of the analyte molecules occurred. This was of great importance for the reusability of the manufactured sensors.

As seen in the graphs, sensor response and recovery dynamics were for acetone than ethanol. For example, when looking at the return times before each sensor was exposed to 20 ppm analytics, for acetone it was 74 s. (PU), 65 s. (PCL) and 76 s. (PLLCL), respectively. Similarly, when examined for ethanol, the return times were 156 s. (PU), 143 s. (PCL) and 99 s. (PLLCL), respectively. The lowest measured concentration was 0.5 ppm and the data showed that the PLLCL-MWNT sensors were capable of detecting 0.5 ppm acetone and ethanol. However, the detection capacity at this low concentration was not observed in other sensors. On the other hand, When the CNT coated gas sensors were exposed to volatile gases, the reaction to ethanol gas was observed to be greater compared to acetone gas based on current change. The reason for this was the high dielectric constant of ethanol (24.5) (Cihat Tasaltın, Fevzi Basarır, 2013) and the ability of CNTs to induce higher conductivity variation. For these reasons, CNT was thought to respond strongly to ethanol.

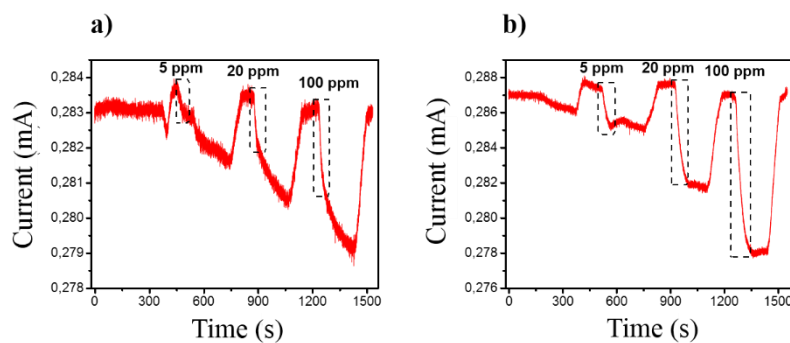


Figure 27. VOC responses of PU-PEDOT:PSS sensor exposed a) to acetone b) to ethanol

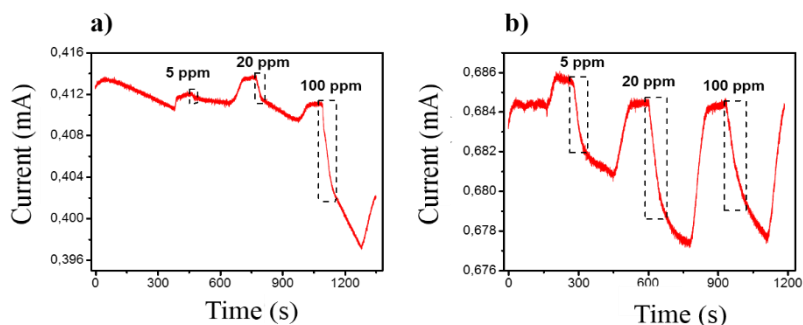


Figure 28. VOC responses of PCL-PEDOT:PSS sensor exposed a) to acetone b) to ethanol

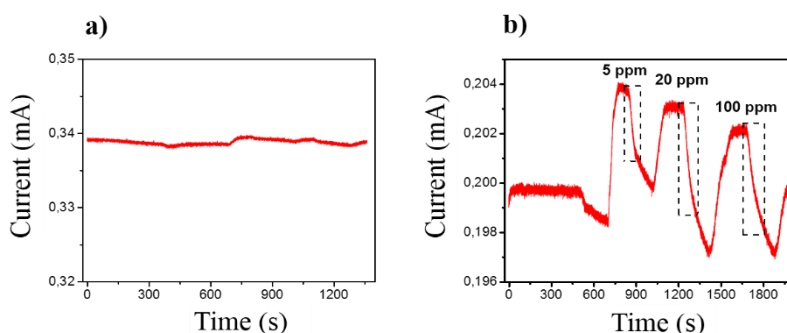


Figure 29. VOC responses of PLLCL-PEDOT:PSS sensor exposed a) to acetone b) to ethanol

In figures 27, 28 and 29, when the time-dependent current changes of PEDOT coated sensors were examined, it was seen that PLLCL-PEDOT: PSS sensor was not sensitive to acetone. In other words, PLLCL-PEDOT: PSS sensor was found to be selective to ethanol. In these three sensors, the reaction against ethanol was higher compared to acetone. This was because ethanol was thought to be associated with the dielectric constant, which is high relative to acetone. According to the literature, polar solvents with higher dielectric constants were found to reduce Coulomb interaction between positively charged PEDOT and negatively charged PSS additives, which increased the hopping rate and conductivity through the screening effect between counter ions and charge carriers (J.Y. Kim et al., 2002). In addition, in a complex environment such as breathing, our analysis was carried out in environments containing humidity 30%, 50% and 70% to understand the effect of “humidity”, the limiting factor.

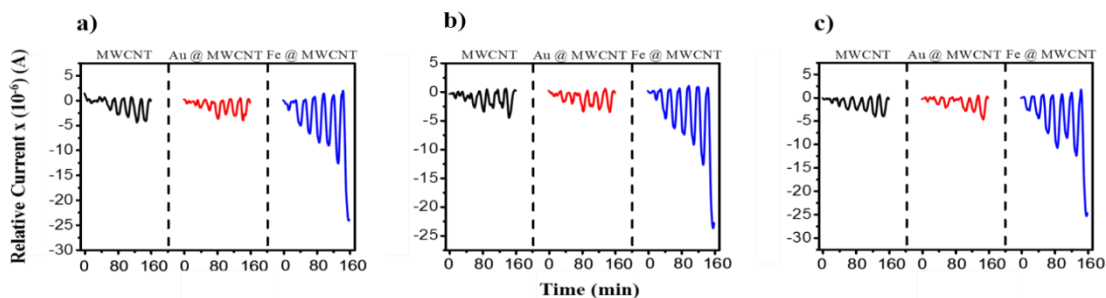


Figure 30. Humid environment acetone response of bare PLLCL-MWCNT, AuNP doped MWCNT and FeNP doped MWCNT sensors in (a) 30%, (b) 50%, and (c) 70% Humid environment.

When the flow graphs (Figure from 30 to 33) of the samples coated with CNT on PLLCL nanofiber against acetone vapor at different percentages of humidity were examined; For CNT sensors decorated with Au nanoparticle, there was no correlation between the increase in humidity concentration and the electrical response. The change in current against the acetone volatile gas of the CNT coated PLLCL nanofibers decorated with Fe nanoparticle was significantly greater compared to the gas sensor samples with bare CNT and decorated Au nanoparticle. As a result of the measurements, it was found that Fe nanoparticle had an accelerator effect on the entry of acetone into the structure. On the other hand, this effect of acetone on Fe nanoparticle Au nano particle was not observed. The reason for this is thought to be the interaction of the free electrons in the carbonyl-bound oxygen of acetone with the Fe surface (Figure 30).

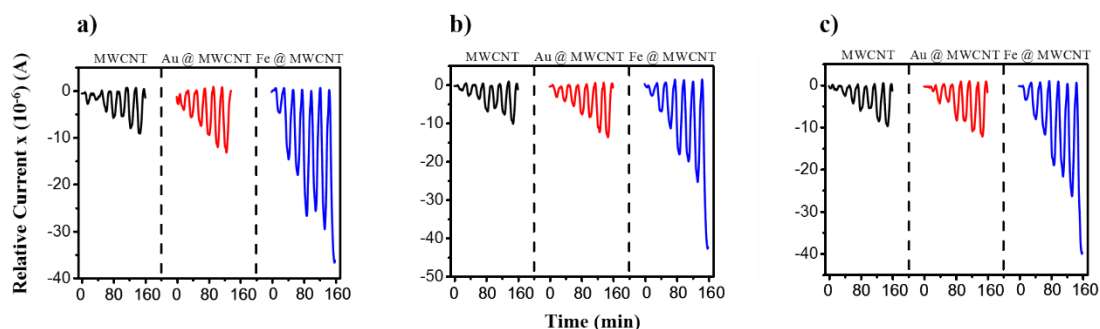


Figure 31. Humid environment ethanol response of bare PLLCL-MWCNT, AuNP doped MWCNT and FeNP doped MWCNT sensors in (a) 30%, (b) 50%, and (c) 66% humid environment.

The electrical response of different percentages of humidity to ethanol vapor of the samples coated with CNT on PLLCL nanofiber was shown in Figure 31. According to the measurements, as the concentration of volatile organic compounds increased, electrical reactivity was observed in all three sensors. As a result of interaction between electron-donating VOCs and negatively doped t- MWCNT, charge carrier densities were changed the conductance of CNTs. Furthermore, due to the charge transfer between VOC and t-MWCNT, it was caused to affect the electrical resistance.

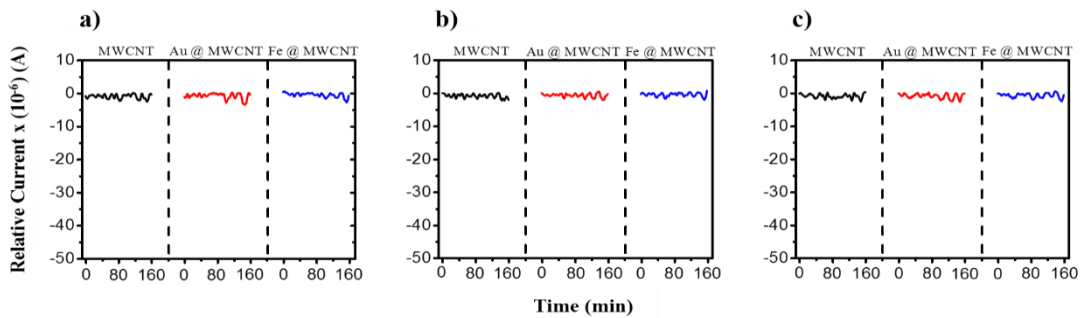


Figure 32. Humid environment toluene response of bare PLLCL-MWCNT, AuNP doped MWCNT and FeNP doped MWCNT sensors in (a) 30%, (b) 50%, and (c) 70% humid environment.

The electrical response of different percentages of humidity to toluene vapor of the samples coated with CNT on PLLCL nanofiber was shown in Figure 32. As a result of the measurements, it was observed that the toluene gas did not react in the samples decorated with nanoparticles in the sensors coated with CNT and in the untreated samples. The nanoparticles were assumed to adsorb toluene vapor and not allow it to reach MWCNT, so no current change was observed.

The electrical response of the samples coated with CNT on PLLCL nano fiber to moisture hexane vapor at different percentages was shown in Figure 33. As a result of the measurements, it was observed that the electrical response to hexane vapor increased in direct proportion with the increase of volatile compound concentration in CNT coated sensors.

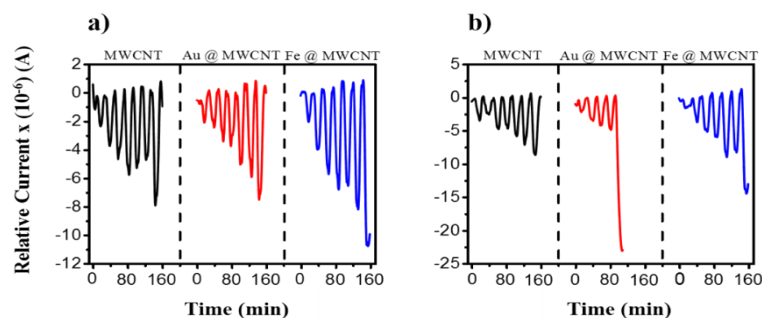


Figure 33. Humid environment hexane response of bare PLLCL-MWCNT, AuNP doped MWCNT and FeNP doped MWCNT sensors in (a) 30%, and (b) 50% humid environment.

Consequently, the electrical response decreased as the moisture percentage increased. The reason for the reduced electrical response was that increased moisture forms a layer on the surface, making it difficult to adsorb gas vapor on the surface.

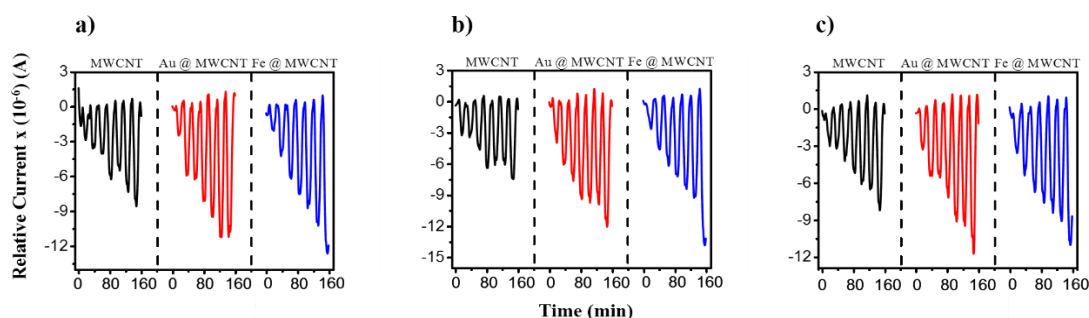


Figure 34. Humid environment isoprene response of bare PLLCL-MWCNT, AuNP doped MWCNT and FeNP doped MWCNT sensors in (a) 30%, (b) 50%, and (c) 70% humid environment.

The electrical response of the samples coated with CNT on PLLCL nanofiber to humidity isoprene vapor at different percentages was shown in Figure 34. When the electrical responses of CNT coated sensors against isoprene vapor were examined, it was observed that they gave the same electrical response as the sensors which were not decorated and decorated with metal nanoparticles. As a result of the measurements, it was seen that isoprene vapor can easily interact with three different surfaces. The electrical selectivity of CNT coated sensors against isoprene vapor was not observed.

However, it was observed to react strongly to isoprene vapors on its three sensors. Some theoretical studies showed strong interaction between CNT and methyl groups (Wen Hui Zao et al., 2012; Sheng Ping Du et al., 2012). So, this strong interaction was thought to be due to the presence of the methyl group in the molecule.

The electrical response of different percentages of humidity of the CNT coated samples on PLLCL nanofiber to chloroform vapor was shown in Figure 35.

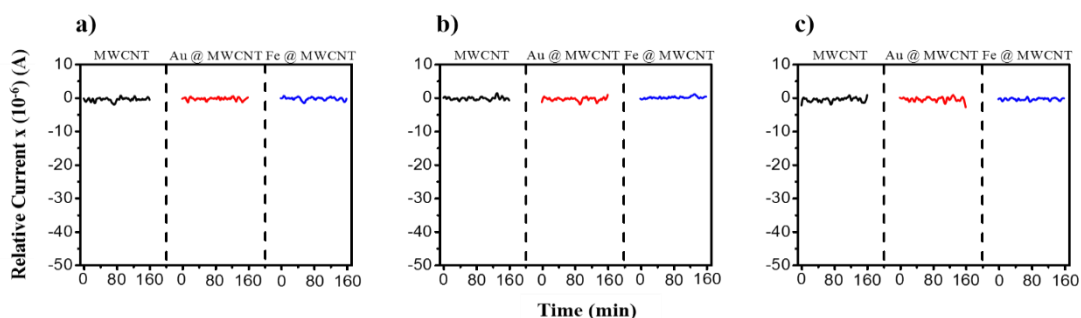


Figure 35. Humid environment chloroform response of bare PLLCL-MWCNT, AuNP doped MWCNT and FeNP doped MWCNT sensors in (a) 30%, (b) 50%, and (c) 70% humid environment

As a result of electrical measurements, it was observed that CNT sensors were unresponsive to chloroform vapor. Chloroform was non-polar like isoprene. It also contained halogen in these two molecules. However, CNT sensors did not react electrically to chloroform vapor. The electrical response to CNT sensors against isoprene vapor was thought to be caused by methyl groups in the isoprene molecule structure. In the chloroform molecule structure, there was no structure in which CNT interacted strongly. So there was no electrical response.

Figures 36 and 37 showed the electrical response of bare PEDOT, Au decorated PEDOT and Fe decorated PEDOT sensors to acetone and ethanol vapors in 30%, 50% and 70% humidity environments.

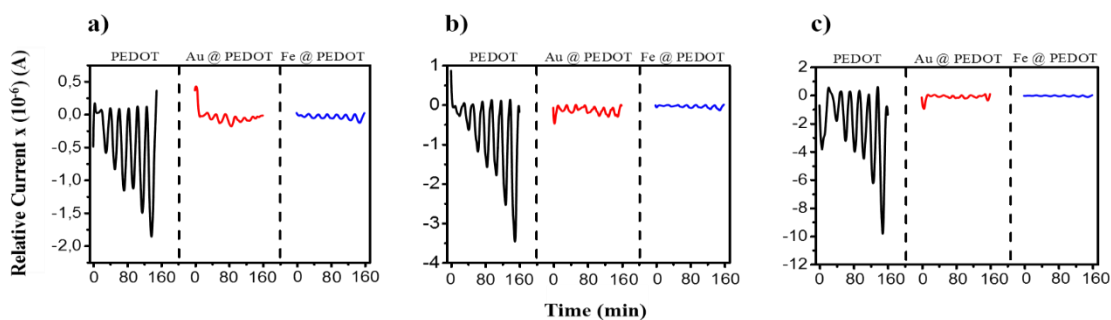


Figure 36. Humid environment acetone response of bare PLLCL-PEDOT, AuNP doped PEDOT and FeNP doped PEDOT sensors in (a) 30%, (b) 50%, and (c) 70% humid environment.

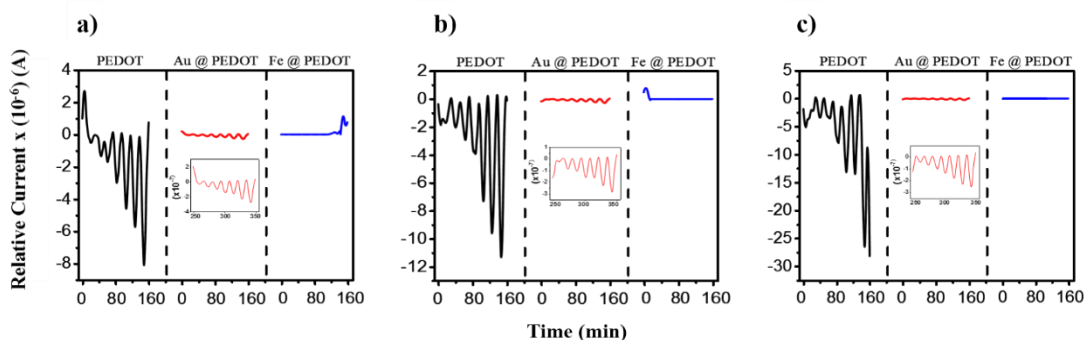


Figure 37. Humid environment ethanol response of bare PLLCL-PEDOT, AuNP doped PEDOT and FeNP doped PEDOT sensors in (a) 30%, (b) 50%, and (c) 70% humid environment.

When the PEDOT sensors were examined, Au decorated PEDOT and Fe decorated PEDOT sensors have little electrical response to ethanol and acetone vapors. Bare PEDOT sensor was more selective against ethanol vapor. In addition, as the humidity increased (from 30% to 70%), the sensor response was lost. Because the diffusion of H₂O into PEDOT:PSS films resulted in swelling of PSS (due to the formation of H₃O⁺ + PSS (SO₃⁻) regions. The swelling of the film increased the distance between adjacent PEDOT-rich areas and caused a reduction in load carrier mobility (Jianyong Ouyang, 2013; Wang et al., 2017). This led to a decrease in conductivity. The response of CNT sensors to volatile organics in humid conditions was superior to PEDOT sensors and their response to hydrophobic gases other than ethanol and acetone has been found to be useful.

CHAPTER 4

CONCLUSION

The purpose of this study was to develop a sensor array to design a next generation volatile analyzer to quantitatively separate VOCs from human breath. The volatile analyzer was successfully produced from PEDOT:PSS and MWCNT coated PLLCL, PU and PCL samples. As a result of its exposure to organic volatile compounds in human breath, this analyzer offered rapid detection capability for point-of-care diagnosis. To increase sensitivity and selectivity, t-MWCNT and PEDOT:PSS coated sensors were doped with AuNP and FeNP. Due to changing the effective surface / volume ratio through NP additive of different sizes, the sensors showed different sensitivity. The proposed nanofiber-based detection platform developed volatile organic compound capture. Thus, the higher surface / volume ratio of nanofibers were allowed for precise detection. These homogeneous nanofibers induce PEDOT and CNT accumulation at the sensing interface, which is critical to sensor performance. PLLCL-PEDOT:the PSS sensor was found to selectively respond to ethanol from 500 ppb to 100 ppm. It was also found that the MWCNT sensing layer was more sensitive to ethanol vapor than acetone. CNT coated gas instruments were found to respond strongly to ethanol. This is due to the fact that ethanol has a higher dielectric constant than acetone and reduces Coulomb interaction between positively charged PEDOT and negatively charged PSS additives. In addition, when CNT sensors decorated with iron nano particles are examined, it is seen that iron nanoparticle has an accelerating effect on the entrance of acetone into the structure. Acetone was thought to be due to the interaction of free electrons in the carbonyl bound oxygen with the Fe surface. When the electrical response of CNT sensors to isoprene vapor was examined, it produced a strong response due to the strong interaction between CNT and methyl groups. In PEDOT sensors, the sensor response is weakened as the amount of humidity increases in the environment. Because the diffusion of H₂O to PEDOT PSS films caused the PSS to swell, and the swelling of the film increased the distance between adjacent PEDOT-rich areas and was thought to cause a decrease in load-bearing mobility.

REFERENCES

- Andre, Rafaela S.; Sanfelice, Rafaela C.; Pavinatto, Adriana; Mattoso, Luiz H.C.; Correa, Daniel S. (2018). Hybrid nanomaterials designed for volatile organic compounds sensors: A review. *Materials and Design* 156 154-166.
[doi:10.1016/j.matdes.2018.06.041](https://doi.org/10.1016/j.matdes.2018.06.041)
- Ahmed, Rania M. (2018). Effect of gold nanoparticles on the physical properties of Poly(3,4-ethylenedioxythiophene):Poly(styrene sulphonate and its gas sensor application. *Arab. J. Nucl. Sci. Appl.*, Vol. 51, 4, 9-18.
[doi:10.21608/ajnsa.2018.2326.1024](https://doi.org/10.21608/ajnsa.2018.2326.1024)
- Badhulika, Sushmee; Myung, Nosang V.; Mulchandani, Ashok. (2014). Conducting polymer coated single-walled carbon nanotube gas sensors for the detection of volatile organic compounds. *Talanta* (2014), 123, 109-114.
[doi:10.1016/j.talanta.2014.02.005](https://doi.org/10.1016/j.talanta.2014.02.005).
- Broza, Y. Y., Vishinkin, R., Barash, O., Nakhleh, M. K., Haick, H. (2018) Synergy between Nanomaterials and Volatile Organic Compounds for Non-Invasive Medical Evaluation. *Chem. Soc. Rev.* , 47, 4781– 4859.
[doi:10.1039/C8CS00317C](https://doi.org/10.1039/C8CS00317C).
- Broza, Y. Y. , and H. Haick. (2013). "Nanomaterial-based sensors for detection of disease." *Nanomedicine* 8 (5):785-806.
- Chen, Minjiao; Qu, Honglin; Zhu, Jiahua; Luo, Zhiping; Khasanov, Airat; Kucknoor, Ashwini S.; Haldolaarachchige, Neel; Young, David P.; Wei, Suying; Guo, Zhanhu. (2012). Magnetic electrospun fluorescent polyvinylpyrrolidone nanocomposite fibers. *Polymer*, 53, 20, 4501-4511.
[doi:10.1016/j.polymer.2012.07.046](https://doi.org/10.1016/j.polymer.2012.07.046).
- Choi, Jaewon; Lee, Jeongwoo; Choi, Jinsub; Jung, Dongsoo; Shim, Sang Eun. (2010). Electrospun PEDOT:PSS/ PVP nanofibers as the chemiresistor in chemical vapour sensing. *Synthetic Metals*, 160, 13-14, 1415-1421.
[doi:10.1016/j.synthmet.2010.04.021](https://doi.org/10.1016/j.synthmet.2010.04.021).
- Compagnone, Dario; Francia, Girolamo Di; Natale, Corrado Di ; Neri, Giovanni; Seeber, Renato; Tajani, Antonella. (2017). Chemical sensors and biosensors in Italy: A review of the 2015 literature. *Sensors*, 17, 868.
[doi:10.3390/s17040868](https://doi.org/10.3390/s17040868).

- Daneshkhah, A., Shrestha, S., Agarwal, M., & Varahramyan, K. (2015). Poly(vinylidene fluoride-hexafluoropropylene) composite sensors for volatile organic compounds detection in breath. *Sensors and Actuators B: Chemical*, 221, 635-643.
[doi:10.1016/j.snb.2015.06.145](https://doi.org/10.1016/j.snb.2015.06.145).
- D'Amico, A.; Bono, R.; Pennazza, G.; Santonico, M.; Mantini, G.; Bernabei, M.; Zarlenga, M.; Roscioni, C.; Martinelli, E.; Paolesse, R., et al. (2008). Identification of melanoma with a gas sensor array. *Skin Res. Technol.*, 14, 226-236.
[doi:10.1111/j.1600-0846.2007.00284.x](https://doi.org/10.1111/j.1600-0846.2007.00284.x).
- Ding, Bin; Wang, Moran; Yu, Jianyong; Sun, Gand. (2009). Gas sensors based on electrospun nanofibers. *Sensors* 9, 1609-1624.
[doi:10.3390/s90301609](https://doi.org/10.3390/s90301609).
- Doshi, J., & Reneker, D. H. (1995). Electrospinning process and applications of electrospun fibers. *Journal of Electrostatics*, 35(2), 151-160.
[doi:10.1016/0304-3886\(95\)00041-8](https://doi.org/10.1016/0304-3886(95)00041-8).
- Du, Sheng-ping; Zhao, Wen-hui; Yuan, Lan-feng. (2012). Absorption and structural property of ethanol / water mixture with carbon nanotubes. *Chinese Journal of Chemical Physics*, 25, 4.
- Ellis, James E; Star, Alexander. (2016). Carbon nanotube based gas sensors toward breath analysis. *ChemPlusChem*, 81, 1248-1265.
[doi:10.1002/cplu.201600478](https://doi.org/10.1002/cplu.201600478).
- Fang, X., Zong, B., Mao, S. (2018). Metal–Organic Framework-Based Sensors for Environmental Contaminant Sensing. *Nano-Micro Lett.*, 10, 64.
[doi: 10.1007/s40820-018-0218-0](https://doi.org/10.1007/s40820-018-0218-0).
- Fenske, J. D., Paulson, S. E. (1999). Human Breath Emissions of VOCs. *J. Air Waste Manage. Assoc.*, 49 (5), 594– 598.
[doi: 10.1080/10473289.1999.10463831](https://doi.org/10.1080/10473289.1999.10463831).
- Galstyan, V., Bhandari, M., Sberveglieri, V., Sberveglieri, G., Comini, E. (2018). Metal Oxide Nanostructures in Food Applications: Quality Control and Packaging. *Chemosensor*, 6, 16.
[doi: 10.3390/chemosensors6020016](https://doi.org/10.3390/chemosensors6020016).
- Garg, K., and G. L. Bowlin. (2011). "Electrospinning jets and nanofibrous structures." *Biomicrofluidics* 5 (1):13403.
[doi: 10.1063/1.3567097](https://doi.org/10.1063/1.3567097).

- Greiner, A., and J. H. Wendorff. (2007). "Electrospinning: a fascinating method for the preparation of ultrathin fibers." *Angew Chem Int Ed Engl* 46 (30):5670-703. doi: [10.1002/anie.200604646](https://doi.org/10.1002/anie.200604646).
- Guntner, Andreas T.; Abegg, Sebastian; Königstein, Karsten; Gerber, Philipp A.; Schmidt-Trucksass, Arno; Pratsinis, Sotiris E. (2019). *Breath Sensors for Health Monitoring*. *ACS Sens.* 4, 268-280. doi:[10.1021/acssensors.8b00937](https://doi.org/10.1021/acssensors.8b00937)
- Haider, Adnan; Haider, Sajjad; Kang Inn-Kyu. (2015). A comprehensive review summarizing the effect of electrospinning parameters and potential applications of nanofibers in biomedical and biotechnology. *Arabian Journal of Chemistry*. doi:[10.1016/j.arabjc.2015.11.015](https://doi.org/10.1016/j.arabjc.2015.11.015).
- Harun, Mohd Hamzah; Saion, Elias; Kassim, Anuar; Yahya, Noorhana; Mahmud, Ekramul. (2007). *Conjugated conducting polymers: A brief overview*. Researchgate, <https://www.researchgate.net/publication/238068724>.
- Hu, J., & Liu, S. (2010). *Responsive Polymers for Detection and Sensing Applications: Current Status and Future Developments*. *Macromolecules*, 43(20), 8315-8330. doi:[10.1021/ma1005815](https://doi.org/10.1021/ma1005815)
- Hui, Yun; Bian, Chao; Xia, Shan hong; Tong, Jianhua; Wang, Jinfen. (2018). *Synthesis and electrochemical sensing application of poly(3,4- ethylenedioxythiophene)-based materials: A review*. *Analytica Chimica Acta* 1022 1-19. doi:[10.1016/j.aca.2018.02.080](https://doi.org/10.1016/j.aca.2018.02.080)
- I. Hafaiedh, W. Elleuch, P. Clement, E. Llobet, A. Abdelghani. (2013). *Multi-walled carbon nanotubes for volatile organic compound detection*. *Sensors and Actuators B* 182 344-350. doi: [10.1016/j.snb.2013.03.020](https://doi.org/10.1016/j.snb.2013.03.020)
- Jalal, A. H., Alam, F., Roychoudhury, S., Umasankar, Y., Pala, N.; Bhansali, S. (2018). *Prospects and Challenges of Volatile Organic Compound Sensors in Human Healthcare*. *ACS Sensors* , 3, 1246– 1263. doi: [10.1021/acssensors.8b00400](https://doi.org/10.1021/acssensors.8b00400).
- Kar, Pradip; Choudhury, Arup. (2013). *Carboxylic acid functionalized multi-walled carbon nanotube doped polyaniline for chloroform sensors*. *Sensors and Actuators B: Chemical*, 183, 25-33. doi: [10.1016/j.snb.2013.03.093](https://doi.org/10.1016/j.snb.2013.03.093)
- Kaushik, Ajeet; Kumar, Rajesh; Arya, Sunil K.; Nair, Madhavan; Malhotra, B. D.; Bhansali, Shekhar. (2015). *Organic-Inorganic hybrid nanocomposite-based gas sensors for environmental monitoring*. *ACS Chem. Rev.* doi:[10.1021/cr400659h](https://doi.org/10.1021/cr400659h)

- Kaushik, Brajesh Kumar, and Manoj Kumar Majumder. (2015). "Carbon Nanotube: Properties and Applications."17-37.
[doi: 10.1007/978-81-322-2047-3_2](https://doi.org/10.1007/978-81-322-2047-3_2).
- Khalili, B.; Boggs, P.B.; Bahna, S.L. (2007). Reliability of a new hand-held device for the measurement of exhaled nitric oxide. *Allergy*, 62, 1171-1174,
[doi:10.1111/j.1398-9995.2007.01475.x](https://doi.org/10.1111/j.1398-9995.2007.01475.x).
- Kim, J.Y; Jung, J.H.; Lee, D.E.; Joo, J. (2002). Enhancement of electrical conductivity of poly(3,4- ethylenedioxythiophene)/poly(4-styrenesulfonate) by a change of solvents. *Synthetic Metals*, 126, 2-3, 311-316.
[doi:10.1016/S0379-6779\(01\)00576-8](https://doi.org/10.1016/S0379-6779(01)00576-8).
- Kim, Il-Doo, Seon-Jin Choi, Sang-Joon Kim, and Ji-Su Jang. (2015). "Exhaled Breath Sensors."19-49.
[doi: 10.1007/978-94-017-9981-2_2](https://doi.org/10.1007/978-94-017-9981-2_2).
- Konvalina, G., Haick Hossam. (2014). Sensors for breath testing: From nanomaterials to comprehensive disease detection. *ACS*, 47, 66-76.
[doi: 10.1021/ar400070m](https://doi.org/10.1021/ar400070m)
- Lang, U., Müller, E., Naujoks, N., & Dual, J. (2009). Microscopical Investigations of PEDOT:PSS Thin Films. *Advanced Functional Materials*, 19(8), 1215-1220.
[doi:10.1002/adfm.200801258](https://doi.org/10.1002/adfm.200801258)
- Lee, J. S., Choi, K. H., Ghim, H. D., Kim, S. S., Chun, D. H., Kim, K. Y., Lyoo, W. S. (2004). Role of molecular weight of atactic poly (vinyl alcohol) (PVA) in the structure and properties of PVA nanofabric prepared by electrospinning. *Appl. Polym. Sci.*, 93, 1638.
[doi: 10.1002/app.20602](https://doi.org/10.1002/app.20602).
- Li, Siying; Chen, Sujie; Zhou, Haoyu; Zhang, Qiuqi; Lv, Yuanmin; Sun, Wenjian; Zhang, Qing; Guo, Xiaojun. (2018). Achieving humidity-insensitive ammonia sensor based on Poly(3,4-ethylene dioxityophene):Poly(styrenesulfonate). *Organic Electronics* 62 234-240.
[doi:10.1016/j.orgel.2018.07.031](https://doi.org/10.1016/j.orgel.2018.07.031)
- Matijević, E.; Scheiner, P. (1978). Ferric hydrous oxide sols: III. Preparation of uniform particles by hydrolysis of Fe (III)-chloride,-nitrate, and-perchlorate solutions. *Journal of Colloid and Interface Science*, 63, 509-524.
- Meyyappan, M. (2016). Carbon Nanotube-Based Chemical Sensors. *Small* (2016) , 12, No.16, 2118-2129

- Mirzaei, Ali; Kim, Jae-Hun; Kim, Hyoun Woo; Kim, Sang Sub. (2018). Resistive-Based gas sensor for detection of benzene, toluene and xylene (BTX) gases: a review. *J. Mater. Chem.C*, 6, 4342.
[doi:10.1039/c8tc00245b](https://doi.org/10.1039/c8tc00245b).
- Mirzaei, A.; Leonardi, S.G.; Neri G. (2016) Detection of hazardous volatile organic compounds (VOCs) by metal oxide nanostructures-based gas sensors: A review. *Ceramics International* 42 15119–15141.
[doi:10.1016/j.ceramint.2016.06.145](https://doi.org/10.1016/j.ceramint.2016.06.145)
- Newsome, Toni E.; Olesik, Susan V. (2014). Electrospinning Silica/Polyvinylpyrrolidone Composite Nanofibers. *Journal of Applied Polymer Science*.
[doi: 10.1002/app.40966](https://doi.org/10.1002/app.40966).
- Ouyang, Jianyong. (2013). Secondary doping” methods to significantly enhance the conductivity of PEDOT:PSS for its application as transparent electrode of optoelectronic devices. *Displays* 34 423–436.
[doi: 10.1016/j.displa.2013.08.007](https://doi.org/10.1016/j.displa.2013.08.007).
- Pavase, T. R.; Lin, H.; Shaikh, Q.-u.-a.; Hussain, S.; Li, Z.; Ahmed, I.; Lv, L.; Sun, L.; Shah, S. B. H.; Kalhor, M. T. (2018). Recent Advances of Conjugated Polymer (CP) Nanocomposite-Based Chemical Sensors and Their Applications in Food Spoilage Detection: A Comprehensive Review. *Sens. Actuators, B*, 273, 1113– 1138.
[doi:10.1016/j.snb.2018.06.118](https://doi.org/10.1016/j.snb.2018.06.118)
- Peng, G., Hakim, M., Broza, Y. Y., Billan, S., Abdah-Bortnyak, S., Kuten, A., Tisch, U.; Haick. (2010). Detection of lung, breast, colorectal, and prostate cancers from exhaled breath using a single array of nanosensors. *H. Br. J. Cancer*, 103, 542– 551.
[doi: 10.1038/sj.bjc.6605810](https://doi.org/10.1038/sj.bjc.6605810)
- Rao, B.Bhooloka. (2000). Zinc oxide ceramic semi-conductor gas sensor for ethanol vapour. *Materials Chemistry and Physics* 64, 62-65.
[doi: 10.1016/S0254-0584\(99\)00267-9](https://doi.org/10.1016/S0254-0584(99)00267-9)
- Righettoni, Marco; Amann, Anton; Pratsinis, Sotiris E. (2015). Breath analysis by nanostructured metal oxides as chemo-resistive gas sensors. *Materials Today*, 18, number 3.
[doi:10.1016/j.mattod.2014.08.017](https://doi.org/10.1016/j.mattod.2014.08.017)
- Rahman, Mohammed M.; Balkhoyor, Hasan B.; Asiri, Abdullah M.; Sobahi, Tariq R. (2016). Development of selective chloroform sensor with transition metal oxide nanoparticle/ multi-walled carbon nanotube nanocomposites by modified glassy

carbon electrode. *Journal of the Taiwan Institute of Chemical Engineers*, 66, 336-346.
[doi: 10.1016/j.jtice.2016.06.004](https://doi.org/10.1016/j.jtice.2016.06.004)

Ramakrishna, S.; Fujihara, K.; Teo, W. E.; Lim, T. C.; Ma, Z. (2005). *An Introduction to Electrospinning and Nanofibers*; World Scientific Publishing Co.: Singapore; Chapter 3, p 90.

Rao, H., Liu, Y., Zhong, J., Zhang, Z., Zhao, X., Liu, X., Wang, Y. (2017). Gold Nanoparticle/Chitosan@N,S Co-doped Multiwalled Carbon Nanotubes Sensor: Fabrication, Characterization, and Electrochemical Detection of Catechol and Nitrite. *ACS Sustainable Chemistry & Engineering*, 5(11), 10926-10939.
[doi:10.1021/acssuschemeng.7b02840](https://doi.org/10.1021/acssuschemeng.7b02840)

Stein, S.E. (1999). An integrated method for spectrum extraction and compound identification from gas chromatography/mass spectrometry data. *Journal of the American Society for Mass Spectrometry*, 10, 770-781.
[doi: 10.1016/S1044-0305\(99\)00047-1](https://doi.org/10.1016/S1044-0305(99)00047-1)

Salehi, Sara; Nikan, Ehsan; AliKhodadadi, Abbas; Mortazavi, Yadollah. (2014). Highly sensitive carbon nanotubes- SnO₂ nanocomposite sensor for acetone detection in diabetes mellitus breath. *Sensors and Actuators B: Chemical*, 205, 261-267.
[doi: 10.1016/j.snb.2014.08.082](https://doi.org/10.1016/j.snb.2014.08.082)

Smith, D., and P. Spanel. (2015). "SIFT-MS and FA-MS methods for ambient gas phase analysis: developments and applications in the UK." *Analyst* 140 (8):2573-91.
[doi: 10.1039/c4an02049a](https://doi.org/10.1039/c4an02049a).

Tasaltın, Cihat; Basarir, Fevzihan. (2014). Preparation of flexible VOC sensor based on carbon nanotubes and gold nanoparticles. *Sensors and Actuators B* 194 173-179.
[doi:10.1016/j.snb.2013.12.063](https://doi.org/10.1016/j.snb.2013.12.063)

Turkevich, J.; Stevenson, P.C.; Hillier, J. (1951). A study of the nucleation and growth processes in the synthesis of colloidal gold. *Discussions of the Faraday Society*, 11, 55-75.

Vaddiraju S., Gleason, K. K. (2010). Selective sensing of volatile organic compounds using novel conducting polymer-metal nanoparticle hybrids. *Nanotechnology*, 21(12), 125503.
[doi:10.1088/0957-4484/21/12/125503](https://doi.org/10.1088/0957-4484/21/12/125503)

Wilson, J. S. (2005). *Sensor Technology Handbook*. In J. S. Wilson (Ed.), *Sensor Technology Handbook* (pp. 1-20). Burlington: Newnes.

- Woellner, M., Hausdorf, S., Klein, N., Mueller, P., Smith, M. W., Kaskel, S. (2018). Adsorption and Detection of Hazardous Trace Gases by Metal-Organic Frameworks. *Adv. Mater.*, 30, 1704679.
[doi: 10.1002/adma.201704679](https://doi.org/10.1002/adma.201704679)
- Wang, Y.; Zhu, C.; Pfattner, R.; Yan, H.; Jin, L.; Chen, S; Lopez, F.M.; Lissel, F.; Liu, J; Rabiah, N.I.; Chen, Z.; Chung, J; Linder, C.; Toney, M.; Murmann, B.; Bao, Z. (2017). A highly stretchable, transparent, and conductive polymer. *Sci. Adv.*, 3.
[doi:10.1126/sciadv.1602076](https://doi.org/10.1126/sciadv.1602076)
- Xiao, Zhuohao; Kong, Ling Bing; Ruan, Shuangchen; Li, Xianglin; Yu, Shijin; Li, Xiuying; Jiang, Yi; Yao, Zhengjun; Ye, Shu; Wang, Chuanhu; Zhang, Tianshu; Zhou, Kun; Li, Sean. (2018). Recent development in nanocarbon materials for gas sensor applications. *Sensors&Actuators:B. Chemical* 274 235 -267.
[doi:10.1016/j.snb.2018.07.040](https://doi.org/10.1016/j.snb.2018.07.040)
- Yucel, M., Akin, O., Cayoren, M., Akduman, I., Palaniappan, A., Liedberg, B., . . . Yildiz, U. H. (2018). Hand-Held Volatilome Analyzer Based on Elastically Deformable Nanofibers. *Analytical Chemistry*, 90(8), 5122-5129.
[doi:10.1021/acs.analchem.7b05187](https://doi.org/10.1021/acs.analchem.7b05187)
- Zhao, Wen-Hui; Shang, Bo; Du, Sheng-Ping; Yuan, Lan-Feng; Yang, Jinlong; Xiao Zeng, Xiao Cheng. (2012) Highly selective adsorption of methanol in carbon nanotubes immersed in methanol - water solution. *The Journal of Chemical Physics*.
[doi: 10.1063/1.4732313](https://doi.org/10.1063/1.4732313)
- Zhang, M.; and Baughman, R. (2011). Assembly of Carbon Nanotube Sheets, Electronic Properties of Carbon Nanotubes.
- Zilberman, Y., Tisch, U., Pisula, W., Feng, X., Müllen, K., & Haick, H. (2009). Spongelike Structures of Hexa-peri-hexabenzocoronene Derivatives Enhance the Sensitivity of Chemiresistive Carbon Nanotubes to Nonpolar Volatile Organic Compounds of Cancer. *Langmuir*, 25(9), 5411-5416.
[doi:10.1021/la8042928](https://doi.org/10.1021/la8042928)